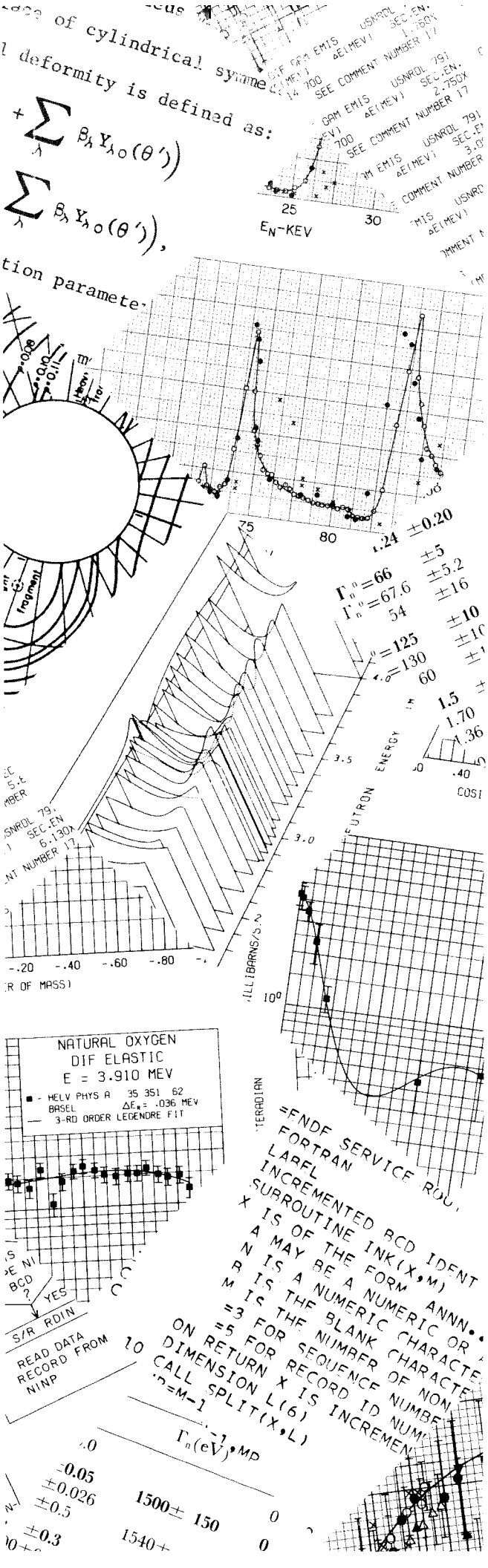

BNL 50379
(ENDF-186)

NEUTRON AND GAMMA RAY PRODUCTION CROSS SECTIONS FOR SILICON

M.R. Bhat, M.D. Goldberg,
R.R. Kinsey, A. Prince,
H. Takahashi

March 1973

BROOKHAVEN NATIONAL LABORATORY
ASSOCIATED UNIVERSITIES, INC.
UPTON, NEW YORK 11973

National Neutron Cross Section Center

BNL 50379
(ENDF-186)
(Physics - TID-4500)

NEUTRON AND GAMMA RAY PRODUCTION CROSS SECTIONS FOR SILICON

M.R. BHAT, M.D. GOLDBERG, R.R. KINSEY,
A. PRINCE, H. TAKAHASHI

March 1973

NATIONAL NEUTRON CROSS SECTION CENTER

BROOKHAVEN NATIONAL LABORATORY

ASSOCIATED UNIVERSITIES, INC.

UNDER CONTRACT NO. AT(30-1)-16 WITH THE

UNITED STATES ATOMIC ENERGY COMMISSION

NOTICE

Printed in the United States of America
Available from
National Technical Information Service
U.S. Department of Commerce
5285 Port Royal Road
Springfield, Virginia 22151
Price: Printed Copy $3.00; Microfiche $0.95

June 1973 1225 copies

Contents

List of Tables

List of Illustrations

1. Introduction

This report describes a reevaluation of silicon neutron and photon production cross-sections data by the National Neutron Cross Section Center. This evaluation was finished in Sept. 1972 and it uses all the data available to the authors up to that time.

In order to put this evaluation in its proper perspective, it seems appropriate to present a brief history of this evaluation. The original evaluation of Si was due to M.K. Drake.[1] This evaluation had both neutron and gamma production cross-section files up to 20.0 MeV. These data files were revised by P.G. Young to conform to data format changes, with additional changes in some of the cross-section data in limited energy regions by R.Q. Wright. To the resulting data files M.K. Drake and R.R. Kinsey[2] added data on $\bar{\mu}_L$, ξ, γ and revised the gamma-production cross-section due to capture. They also modified the cross-section for the production of the 1.779 MeV gamma-ray to reflect the changes made by R.Q. Wright in the corresponding inelastic cross-section. This evaluation was later assigned a MAT No. = 1151 and became part of the ENDF/B-III data library. The present evaluation RSIC No. 4151, Mod. 2 is based on this evaluation by Drake and Kinsey with extensive modifications which will be described in detail in the following pages. A brief summary of these changes along with the history of this evaluation is given in a tabular form below. If there is no reference to changes in a specific cross-section in this report, it is to be understood that the corresponding data files are the same as in the ENDF/B-III evaluation.

History of the Silicon Evaluation

Author	Description and or Revisions	Report
M.K. Drake	Original evaluation with neutron and gamma production files up to 20 MeV	GA-8628 (DASA-2099) May 1, 1968
P.G. Young	Revised for format changes	
R.Q. Wright	Total and elastic cross-sections revised 1.8-3.62 MeV Added non-elastic cross-section Total inelastic and inelastic cross-section to the 1.779 MeV level revised between 1.85-3.53 MeV Elastic angular distribution given as Legendre coefficients	
M.K. Drake and R.R. Kinsey	Sections on $\bar{\mu}_L$, ξ, γ added Gamma production cross-sections due to capture revised Cross-sections for the production of the 1.779 MeV gamma ray by inelastic scattering changed to agree with the corresponding changes in the inelastic scattering cross-section made by R.Q. Wright This Evaluation was given MAT NO = 1151 and is part of the ENDF/B-III Library	ENDF/B Summary Documentation ENDF-201
Authors of this Report	Total cross-section data replaced by new NBS data from 0.5-20 MeV Elastic, non-elastic, total inelastic and partial inelastic cross sections changed to conform to new total cross-section data (n,α) cross-section reevaluated from 8.4-20.0 MeV $\bar{\mu}_L$, ξ, γ, files changed New Legendre coefficients for elastic and inelastic scattering data added Gamma production cross-sections due to inelastic scattering recalculated Energy distribution of secondary photons recalculated using a statistical model The data files resulting from these modifications on the MAT = 1151 evaluation were given an RSIC No. = 4151, Mod 2 and sent to RSIC on Sept. 20, 1972	This Report ENDF-186 BNL-50379 March 1973

2. General Properties of Silicon Isotopes

2.1 Isotopic Mass and Possible Neutron Induced Reactions

Natural silicon is made up of three isotopes - ^{28}Si, ^{29}Si and ^{30}Si. Their fractional abundances and isotopic masses are given in Table 1. One can readily see that the properties of natural silicon are essentially determined by ^{28}Si. The nuclear masses are from the compilation of Wapstra and Gove.[3] In Table 2 we give the Q values for the different possible nuclear reactions up to a maximum neutron energy of 20 MeV. These were also calculated using the same mass tables. Since some of these reactions viz: (n,t), (n,^{3}He) and (n,nα) were found to make very small contributions, they were ignored in the evaluated data set. From this Table we note that the Q-value for the (n,α) reaction for a mixture of isotopes should be 33.1 kev whereas in the ENDF/B-III version it is given as 32.7 kev. Since they are so close the Q-value was left unchanged at 32.7 kev. Rest of the (n, particle) data files were not changed.

2.2 Energy Levels of the Silicon Isotopes

The energy levels of the three silicon isotopes, along with their spins and parities, are given in Figs. 1-3. These constitute the result of some of the latest work on the level schemes of these isotopes and is mostly due to the experimental work in Refs. 4-10. The level schemes are essentially the same as used in the original Drake evaluation with a few minor changes in level energies and spin assignments. These level schemes were used in the nuclear model calculations for the different reaction cross-sections to be described later.

2.3 Discrete Gamma Rays Produced by Neutron Interactions

The discrete gamma rays produced by $(n,n'\gamma)$ reactions in the Si isotopes are also shown in Figs. 1-3. In Tables 3-5 we give a list of these gamma rays along with the initial and final nuclear states and their transition probabilities. This information is taken from the Drake report with a few minor modifications and is due to the data in Refs. 11-23. This data is needed for calculating the gamma production cross-sections due to inelastic scattering as will be described later on.

In Table 6 we give a list of the gamma rays originating from thermal neutron capture in silicon along with their multiplicities. This data is from the work of Spits et. al.,[10] Lycklama et. al.[24] and by Blichert-Toft and Tripathi.[25] This is the experimental data used to derive the gamma production cross-section due to neutron capture. At higher neutron energies, the experimental data of Lundberg and Bergqvist[26] at 68 kev was used.

3. Neutron Cross Sections

3.1. The Total Cross Section

The total neutron cross-section data used in the original Drake and ENDF/B-III evaluations are described in detail in the earlier report.[1] In the present evaluation we have changed the total cross-section data in the energy interval 0.5-20.0 MeV using the NBS data of Schwartz et. al.[27] Another set of total cross-section data of comparable quality is that due to Cierjacks et. al.[28] from Karlsruhe. On comparison of these two sets of data, it was found that the Karlsruhe data gave a higher cross-section in general. Thus at 8.7 MeV the Karlsruhe data is 6.8% higher than the NBS data, pointing to some possible problems with background subtraction. Hence, it was decided to use the NBS data which has a statistical error of about 3% at the lower end of the energy scale and about 4% at the higher end. The data points naturally are very closely spaced at the lower end of the energy scale and they become sparser as one goes up in energy. The scatter in the energy points also becomes large at the higher end of the scale and the experimental data does not show any well-defined structure above 12.0 MeV. In order to obtain a smooth curve passing evenly amongst the data points a spline fit was made to the data points using a program SPLIN written by D.E. Cullen.[29] In this program one has to specify the abscissa and ordinates of a certain number of nodes to obtain the corresponding spline fit. By trial and error one can determine the nodes needed to have a curve passing through the experimental points and reproduce faithfully the general trend of the experimental data. One result of such a fit is shown in Figs. 4-7 where the curve indicates the total cross-section in the ENDF/B files obtained from the spline fit and the points are the NBS experimental data. Above

12.0 MeV, because of the large spread in the data, the experimental points were averaged over one MeV energy intervals and the mean value given at the mid-point of the energy range. This essentially gives a constant cross-section without any structure at the high energy end of the scale.

3.2. The (n,α) Cross-Section

The (n,α) cross-section was left unchanged up to 8.4 MeV as given in the ENDF/B-III evaluation. Above this energy it was re-evaluated to conform to some recent experimental data. These changes are discussed in the following.

Above 8.4 MeV, there are no measurements of the (n,α) cross-section for ^{28}Si. There are, however, some experimental data for the (n,α) cross-section of ^{30}Si. Hence, use was made of the theoretical calculations of Gardner and Yu[30] which give the ratio of the (n,α) cross-sections of ^{28}Si, ^{29}Si and ^{30}Si. These calculations are based on a statistical model and give the relative cross-sections of the isotopes of an element as a function of the incident particle energy, the Q-value of the reaction, the level density and the pairing energy of the daughter nucleus. The ratios of the (n,α) cross-sections for the silicon isotopes at about 14 MeV as calculated by these authors are:

$$^{28}Si:^{29}Si:^{30}Si = 1.00:1.27:0.485 .$$

The experimental values for ^{30}Si (n,α) cross-section available at the time of the Drake evaluation were: Paul and Clarke[31] 45.9 ± 25.0 mb at 14.5 MeV; Khurana and Govil[32] 123.0 ± 15.0 mb at 14.8 MeV and Pasquarelli[33] 175.0 ± 18.0 mb at 14.7 MeV. Since then, two additional values have been published viz. Ranakumar et. al.[34] 68.0 ± 8.0 mb at 14.4 MeV and Singh[35] 73.6 ± 10.3 mb at 14.5 MeV. Adopting the two newer values which are in

good agreement, we take a weighted average to give 70.5 mb for the (n,α) cross section of ^{30}Si.

If the calculated ratios of Gardner and Yu given above and this value for the (n,α) cross-section for ^{30}Si are used, one obtains for ^{28}Si $\sigma(n,\alpha)$ = 145.4 mb and for ^{29}Si $\sigma(n,\alpha)$ = 184.6 mb. However, this result is at variance with the experimental data of Andersson-Lindström[36] who measured ^{28}Si $\sigma(n,\alpha)$:^{29}Si $\sigma(n,\alpha)$ ratio as 8.5 ± 1.2 at 14.5 MeV. Hence, as a way out of this contradiction, it is assumed that Gardner and Yu's theoretical calculations are likely to be more realistic in a comparison between even-even nuclei i.e. ^{28}Si and ^{30}Si rather than between even-even and even-odd nuclei i.e. ^{28}Si and ^{29}Si. Therefore using the Andersson-Lindström ratio of 8.5 and the ^{28}Si (n,α) cross-section to be 145.4 mb the corresponding cross-section for ^{29}Si is found to be 17.1 mb. Thus, one obtains the final values adopted in this evaluation at a nominal energy of 14.5 MeV as: ^{28}Si $\alpha(n,\alpha)$ = 145.4 mb, ^{29}Si $\alpha(n,\alpha)$ = 17.1 mb and ^{30}Si $\alpha(n,\alpha)$ = 70.5 mb.

These cross-sections weighted with the natural abundances of the respective isotopes give the (n,α) cross-section for natural Si as 137.1 mb at 14.5 MeV. It should be noted here that if the much higher value of 184.6 mb had been adopted for the ^{29}Si (n,α) cross-section as given by the Gardner and Yu ratio, the cross section of silicon would be 145.0 mb. This is only 5.8% higher than 137.1 mb and is well within the uncertainties of the cross-section. The (n,α) cross-section for natural silicon as given in the Drake evaluation[1] is 246.5 mb at 14.5 MeV. The new value adopted in this evaluation is about 44% lower indicating a newer set of cross-section values between 8.4 and 20.0 MeV.

At the time of the previous evaluation, several data sets existed in which measurements were made giving the cross-section versus energy for the

production of various alpha groups. Since ^{28}Si is the dominant isotope, all the alphas are ascribed to the α_0, α_1, α_2.....etc. groups of this isotope. Such data existed from several separate measurements for neutron energies up to 8.4 MeV. The previous evaluation considered each experiment in detail and provided a composite total alpha production cross-section for ^{28}Si which was then defined as the total (n,α) cross-section for natural silicon from threshold to 8.4 MeV.

Since then, another study of this reaction has been published by Grimes.[37] The total elastic (at two angles - 15° and 30°), (n,p_{0+1}), (n,p_{2+3}), (n,α_0), (n,α_1), (n,α_2) and (n,α_3) cross-sections were measured between 6.64-13.44 MeV. The measurements of the (n,p_i) and (n,α_i) reactions were made simultaneously with a silicon surface barrier detector serving as both the target and the detector. The normalization was thus internal and effectively to the total cross-section. A plot of the sum of (n,α_0), (n,α_1), (n,α_2) and (n, α_3) production cross-sections of Grimes between 6.64 and 8.4 MeV when compared to the natural silicon (n,α) cross-section of the Drake evaluation indicates excellent agreement with respect to both the absolute magnitude and the structure of the cross-section.

The structure in the Grimes data continues above 11.0 MeV, but the sum cross-section is no longer the total production cross-section since α_4, α_5 etc. are not accounted for tthough clearly seen in the spectra. Thus, at 13.44 MeV the "sum" cross-section value is about 35 mb as compared to the 137.1 mb "best value" at 14.5 MeV recommended in this evaluation. Hence, it is concluded that the (n,α) curve of the previous evaluation still represents adequately the (n,α) cross-section from the threshold to 8.4 MeV.

Using the 207.6 mb value at 8.4 MeV from the previous evaluation and 137.1 mb at 14.5 MeV arrived at in this evaluation, a smooth curve was

drawn to represent the average natural silicon (n,α) cross-section. This curve rises to a maximum of about 269 mb at about 10.6 MeV. The curve was then continued above 14.5 MeV to 20.0 MeV by a linear extrapolation on a semi-log plot. The ratio of the 14.5 MeV and 20.0 MeV values were made as close as possible to the same ratio of the (n,α_0) reactions as measured by Rubbino and Zubke.[38] The resulting curve of the (n,α) cross-section as given in the present evaluation is shown in Fig. 23.

3.3. Inelastic Scattering Cross-Section

Adoption of new total cross-section and (n,α) data as described constitute two of the major changes in the present silicon evaluation as compared to its earlier versions. Since there was no significant new data to warrant extensive changes in the other cross-sections, it was decided to keep the rest of the (n,γ) and (n, particle) cross-sections unchanged. However, the elastic and inelastic scattering cross-sections to the various excited states of the silicon isotopes had to be changed in conformity with changes in the total cross-section. The procedure adopted for such changes is described below.

Nuclear model calculations were made using the ABACUS-2 optical model code[39] and Greenlees[40] parameters which are given in Table 7. The level excitation energies and their spins and parities used in these calculations are given in Figs. 1-3. Such calculations give, total, elastic and inelastic scattering cross-sections for the three silicon isotopes. A sum of these calculated total cross-sections weighted according to the isotopic abundance would give us a "total" cross-section containing no (n, particle) cross-sections or the (n,γ) cross-section. Hence, the results of the optical model calculations were normalized by multiplying them by the ratio

$$\frac{\sigma_{\text{Total (expt)}} - \Sigma\, \sigma_{(n,\ \text{particle})} - \sigma_{(n,\gamma)}}{\sigma_{\text{"Total" (calc)}}}$$

as a function of the neutron energy. In particular, this ratio was used to normalize the inelastic scattering cross-sections to the individual levels in the three isotopes of silicon. These were the first 12 levels in ^{28}Si up to an energy of 8.260 MeV, the first 5 levels in ^{29}Si up to an energy of 3.623 MeV and the first 4 levels in ^{30}Si up to an energy of 3.788 MeV. The assumptions underlying such a normalization procedure are firstly that of an extreme compound nucleus picture and secondly that the relative magnitudes of the different inelastic cross-sections are given by the optical model calculations. The result of such a normalization is to obtain a set of inelastic cross-sections to the different excited states with the same kind of fine structure as in the total cross-section "built in". It is interesting to compare these cross-sections with experimental data available for the 1.779, 4.617, 4.975 and 6.276 MeV levels in ^{28}Si. There are no experimental data for the excitation cross-sections to any other levels. As of this writing the most extensive data is for the 1.779 MeV level in ^{28}Si. The experimental data plotted against the normalized curve is shown in Fig. 14 from the threshold to 5.0 MeV and in Fig. 15 from 5.0 to 10.0 MeV. The experimental data is from Refs. 41-51. In such a comparison one must bear in mind the fact that data on inelastic excitation functions is measured with a much broader neutron energy resolution than the total cross-section data. This is indicated by the horizontal error bars about each data point. The vertical bars indicate the error in the value of the cross-section. Where such bars are absent, either these uncertainties have not been quoted by the authors or they are of the order of the size of the corresponding

symbols. Looking at the trend of the calculated cross-section and the experimental points, the agreement is good except in the case of the 1961 Lind and Day data at low energies which are consistently lower. The high resolution inelastic cross-section data for the 1.779 MeV level from threshold to 3.53 MeV given in Ref. 52 could not be used as it was not available in the final form at the time of the evaluation. In the case of 4.617 MeV level (Fig. 16) a comparison of the available experimental data with the normalized curve indicates that the experimental data are lower by nearly a factor of 2. For the 4.975 and 6.276 MeV levels (Figs. 17 and 18) the agreement between experiment and the evaluated curves is satisfactory.

As mentioned earlier, the inelastic scattering cross-sections for a total of 21 levels in the three isotopes of silicon have been given in the evaluated data files. The remaining inelastic scattering cross-sections to some 46 remaining nuclear levels were lumped together as a cross-section for scattering into the continuum (MF = 3, MT = 91). This cross-section is shown in Fig. 19. It should be mentioned here, as a point of detail, that the energy grid used in normalizing the different partial cross-sections was the same as that used to give the total cross section. This simplifies to a considerable extent the whole procedure and one is assured of an energy grid which is fine enough to accommodate the structure in the different cross-sections.

3.4. The Elastic Scattering Cross-Section

A sum of all the inelastic scattering cross-sections, the (n, particle) cross-sections and the capture cross-section when subtracted from the total cross-section determined from the experimental data gives us the elastic scattering cross-section. It is interesting to compare this cross-section

with experimental data where available. Such a comparison from 0.5-11.0 MeV is shown in Fig. 8. The experimental data are due to the workers in Refs. 43, 46, 49, 50, 53-56. The horizontal bars associated with each data point indicate the neutron energy resolution and the vertical bars the data errors. The agreement between the experimental data and the evaluated curve is good especially if one bears in mind the broad neutron energy resolution of the individual data points.

4. Angular Distribution of Secondary Neutrons

4.1. Elastically Scattered Neutrons

The angular distributions of the elastically scattered neutrons were given in the original Drake evaluation as normalized probability distributions. These were converted to give the corresponding Legendre polynomial expansion coefficients using the code CHAD.[57] The experimental data sets used have been tabulated in the original report.[1] In addition, some of the new data by Knitter and Coppola,[46] Kinney and Perey[50] were used. The experimental data of the last reference for E_n = 8.56 ± 0.08 MeV and a Legendre polynomial fit of order eight are shown in Fig. 27. A value of about 980 mb/sr was used in the forward direction and between 140° and 180°, the experimental points were supplemented by points read off from the dashed curve given in this reference. In fitting the data for differential elastic scattering, consistency checks with Wick's limit were made. It was also made sure that the Legendre polynomial expansion coefficients reproduced a non-negative differential elastic scattering cross-section.

In addition, new files giving $\bar{\mu}_L$, ξ and γ were generated using the code[58] DUMMY5 and plots of these are shown in Figs. 24-26.

4.2 Inelastically Scattered Neutrons

The angular distribution of inelastically scattered neutrons for the 1.779 MeV level of ^{28}Si were converted to the corresponding Legendre polynomial expansion coefficients and are included as such in the evaluated data files. In addition to the data in the Drake evaluation, new data by Kinney and Perey[50] has been used. A fit made to the E_n = 7.55 ± 0.04 MeV and E_{ex} = 1.779 MeV data from this reference using CHAD is shown in Fig. 28.

It should also be mentioned here that coupled channel calculations were carried out to determine the direct contribution due to the coupling of the first two excited states of each silicon isotope to account for the anisotropy of the differential inelastic scattering. However, since the experimental data showing such anisotropy were sparse, it was decided not to use these calculations.

5. Gamma Ray Production Cross Sections

5.1. Production of Radiative Capture Gamma Rays.

a. Low Energy Capture (10^{-5} eV - 50 keV)

The energies and multiplicities for the gamma rays due to neutron capture in this energy range were obtained from the thermal neutron capture data of Spits et al.,[10] Lycklama et al.[24] and Blichert-Toft and Tripathi.[25] These data are given in Table 6, with gamma ray energies, their multiplicities, energy of the initial state as well as the isotopic identification of the target nucleus. The binding energies of neutrons in the compound nuclei resulting from neutron capture in ^{28}Si, ^{29}Si and ^{30}Si are 8,474.2 ± 0.5 kev, 10,609.9 ± 1.0 kev and 6589.1 ± 0.7 kev respectively. However, an effective binding energy of 8,767.6 kev for silicon as recommended by Orphan et. al.[60] has been used in this evaluation. The experimental data given in Table 6 was therefore normalized to this Q-value for the (n,γ) reaction.

b. High Energy Capture (above 50 kev)

For this neutron energy range, the experimental data of Lundberg and Bergqvist[26] at 68 keV are used. The measurements in this work were done with a NaI(Tl) scintillator and as such, the gamma ray energies are given with a broader energy resolution as compared to a Ge(Li) detector. By comparison with Ge(Li) detector data of thermal neutron capture, it was possible to establish a plausible one-to-one correspondance between the gamma ray energies given by Lundberg and Bergqvist and the Ge(Li) detector measurements. The multiplicities of the 68 keV measurements were used and if a gamma ray was known to be a primary transition, the kinetic energy of the neutron was added to the gamma-ray energy to satisfy energy conservation. The multiplicities and the gamma ray energies are given starting from 0.1 MeV neutron energy in steps of 0.1 MeV up to 1.0 MeV. Above this neutron energy,

the gamma spectrum is treated as a continuum and only average multipicities are given in File 12 (MF=102) and the energy distribution of the gamma spectrum is given in File 15. These energy distributions were obtained by putting all the discrete gamma rays in gamma ray energy bands 0.5 MeV wide to give a histogram.

5.2 Cross Sections for the Production of $(n,n'\gamma)$ Gamma Rays

The data on the gamma rays and their transition probabilities given in Tables 3-5 was used to calculate the gamma production cross-section due to inelastic scattering from the corresponding inelastic scattering cross-sections. In these calculations, gamma rays originating from levels less than or equal to the 8.260 Mev level in ^{28}Si, the 3.623 MeV level in ^{29}Si and the 3.788 MeV level in ^{30}Si were explicitly treated as discrete gamma rays and their production cross-sections calculated. Since excited states lying above the three energies in the corresponding isotopes were treated as part of the "continuum"; the gamma rays originating in these levels were treated differently as described below. If the transition probabilities of the different gamma rays are known, it is possible to follow in detail, the number populating a particular state and the number depleting such a population and calculate the gamma production cross-sections. Since, the resulting cross-sections had a lot of fine structure in them, they were averaged over 20 kev intervals from the threshold up to 5.0 Mev, and over 200 kev intervals to 10.0 MeV and over 1.0 Mev intervals up to 20.0 MeV. These cross-sections were calculated up to 20.0 MeV for some of the gamma transitions in ^{28}Si where data on the production cross-section were available at energies above 10.0 Mev; otherwise then cross-sections were calculated only up to 9.0 Mev in ^{28}Si and up to 4.0 MeV in ^{29}Si and ^{30}Si. The

experimental data on the production cross-sections is due to Tucker et al.[61], Drake et al.[62] and other experimental data given in Ref. 61. A comparison between the calculated curves and the experimental data is shown in Figs. 29-39. The neutron energy resolution is shown by a horizontal bar, otherwise it is less or equal to the horizontal extension of the symbol. It should be emphasized here that the calculated curves have not been normalized to any experimental value. The agreement between the calculated curves and the experimental data is good, especially for the more intense gamma rays.

The photons not treated as discrete gamma rays were accounted for by assuming that they form part of a continuous gamma spectrum. This is the case with those discrete gamma rays whose cross-sections are given only up to 9.0 MeV. However, cross-sections of some of the more intense gamma rays are given up to 20.0 MeV. Hence, the following procedure (suggested by M.K. Drake) was used to subtract the contributions of the discrete gamma rays. It is assumed that the gamma production cross-section at 9.0 MeV is 1.48b and at 14.5 MeV is 1.75b[1]. The ratio of the total gamma production cross-section to the non-elastic cross-section (this is the yield or the multiplicity $y(E_n)$) is found to be 1.23 at 9.0 MeV and 1.60 at 14.5 MeV. It was assumed that a straight-line interpolation could be made between 9.0 and 14.5 MeV to obtain this ratio at points in between and that one could extend the straight line to get this ratio up to 20.0 MeV. The recommended non-elastic cross-section multiplied by this ratio thus gives the total gamma production cross-section. The energy distribution of the continuum photons, $\frac{d\sigma\gamma}{dE\gamma}(E_\gamma \leftarrow E_n)$ as well as the average photon energy $\overline{E}_\gamma (E_n)$ averaged over this energy distribution were calculated using the GRØGI-III Code,[63] as described in the next section. The total energy released per reaction as photons is $\overline{E}_\gamma (E_n) \times y (E_n)$. From this the total

gamma ray energy E_γ^D released as discrete photons (this is obtained by averaging $E_{\gamma i}$ for the i-th discrete gamma over its corresponding production cross-section $\sigma_{n,xi}$) is subtracted to give gamma energy E_γ^C appearing in the continuum. This is used to calculate the photon production cross-section for the continuum as

$$\sigma_{n,\ x\gamma}^{C}(E_n) = \frac{E_\gamma^C(E_n)}{E_\gamma(E_n)}\ \sigma_{n,x}(E_n)$$

The normalized energy distribution for the continuum is also given in File 15.

5.3 Energy Distribution of the Secondary Gamma Rays

In discussing capture gamma ray spectra it was mentioned how gamma rays due to capture above 1.0 MeV neutron energy were grouped together into bins 0.5 MeV wide and the distribution normalized to give an energy distribution of the gamma ray spectrum.

The gamma-ray production cross-sections, its energy distribution and mean energy were calculated from 9.0 to 20.0 MeV. Neutron energy using the GRØGI-III. Code.[63] Since ^{28}Si is the dominant isotope calculations were made only for ^{28}Si. In this code, cascade calculations based on a statistical theory are performed to estimate contributions from the different gamma rays. In these calculations, the level-density formula used is that of Gilbert and Cameron[64] The level density parameters for the parent nucleus and the different daughter nuclei produced in the cascade processes were all taken from this paper and are listed in Table 8. At high excitation energies involving high nuclear spin values the relative importance of γ versus particle emission has to be properly calculated using the yrast levels. The yrast levels for high spin were calculated using the prescription given in the paper of Gilat[65] and Grover and Gilat[66] and the compilation of Endt and Van der Leun[17]. These data are

given in Table 9 in MeV. The binding energies of neutron, proton and α-particles for all nuclei are given in Table 10 in MeV. All data except for ^{21}Ne were taken from the previous reference. The data for ^{21}Ne are from Mattauch et al.[67] The transmission coefficients for n, p and α particles were calculated using ABACUS-2 using the optical model parameters of Becchetti and Greenless[40]. The optical model parameters for the α particles are from Huizenga and Igo[68]. The GRØGI-III Code calculates the gamma spectrum from each cascade process. The total gamma production cross-section as well as the energy distribution of the gamma spectrum were obtained by summing all these contributions.

Acknowledgement

It is a great pleasure to express our thanks to our colleagues at the NNCSC; especially M. K. Drake who apart from discussions and suggestions regarding this work, patiently explained and clarified the formats and procedures for the photon production files. We are also grateful to D.E. Cullen for writing the codes for the spline fit and plotting, and to A. J. Fuoco for help in plotting the data.

References

1. M. K. Drake Neutron and Gamma Ray Production Cross Sections for Silicon DASA 2099, GA-8628, May 1, 1968.

2. M. K. Drake and R. R. Kinsey, Summary Documentation on the ENDF/B-III Si Evaluation ENDF-201 (To be Published).

3. A. H. Wapstra and N. B. Gove Nuclear Data Tables 9, 265, 1971.

4. F. C. P. Huang, E. F. Gibson and D. K. McDaniels Phys. Rev. C3, 1222, 1971.

5. Gerhard J. Wagner Nucl. Phys. A176, 47, 1971.

6. S. T. Lam, A. E. Litherland and R. E. Azuma, Can. J. of Phys. 49, 685, 1971.

7. I. G. Main, N. Dawson, C. K. Davies, G. D. Jones, P. J. Mulhern, V. E. Storizhko, R. D. Symes, M. F. Thomas and P. J. Twin, Nucl. Phys. A158, 364, 1970.

8. T. T. Bardin, J. A. Becker, T. R. Fisher and A. D. W. Jones Phys. Rev. C4, 1625, 1971.

9. R. D. Symes, B. E. Crossfield, N. Dawson, G. D. Jones, I.G. Main, P. J. Mulhern, M. F. Thomas and P. J. Twin, Nucl. Psys. A167, 625, 1971.

10. A. M. J. Spits, A. M. F. Op Den Kamp and H. Gruppelaar Nucl. Phys. A145, 449, 1970.

11. T. K. Alexander AECL-2610, p10, 1966.

12. R. J. A. Levesque, R. W. Ollerhead, E. W. Blackmore and J.A. Kuehner Can. J. Phys. 44, 1087, 1966.

13. T. K. Alexander, AECL-2639, p14, 1966.

14. R. Nordhagen, M. Hoffman, F. Ingebretsen and A. Tveter, Phys. Lett. 16, 163, 1965.

15. A. E. Litherland, T. K. Alexander and P. J. M. Smulders, AECL-2612, p10, 1966.

16. J. I. Valerio and E. B. Nelson, Nucl. Phys. 29 70, 1962.

17. P. M. Endt and C. Van der Leun, Nucl. Phys. A105, 1, 1967.

18. T. W. Retz - Schmidt, S. J. Skorka, J. Morgenstern and H. Schmidt, Phys. Lett. 16, 280, 1965.

19. S. J. Skorka, T. W. Retz-Schmidt, H. Schmidt, J. Morgenstern and D. Evers Nucl. Phys. 68, 177, 1965.

20. T. K. Alexander et. al. AECL-2612, p10, 1966.

21. S. I. Baker, R. E. Segel Bull. Amer. Phys. Soc. 12, 570, 1967.

22. H. J. Hausman, W. E. Davis, C. V. Philips, R. P. Sullivan and G. R. Unrine Phys. Rev. 148, 1136, 1966.

23. P. J. M. Smulders Phys. Lett. 9, 155, 1964.

24. H. Lycklama, L. B. Hughes and T. J. Kennett Can. J. Phys. 45, 1871, 1967.

25. P. H. Blichert-Toft and K. C. Tripathi Symp. on Neutron Capture Gamma Ray Spectroscopy, Studsvik. IAEA, Vienna, 1969 STI/Pub/235.

26. B. Lundberg and I. Bergqvist Physica Scripta 2, 265, 1970.

27. R. B. Schwartz, R. A. Schrack and H. T. Heaton Bull. Am. Phys. Soc. 16, 495, 1971.

28. S. Cierjacks, P. Forti, D. Kopsch, L. Kropp, J. Nebel and H. Unseld. KFK-1000, 1968.

29. D. E. Cullen, Private Communication, 1972.

30. Donald G. Gardner and Yu-Wen Yu Nucl. Phys. 60, 49, 1964.

31. E. B. Paul and R. L. Clarke Can. Jour. Phys. 31, 267, 1953.

32. C. S. Khurana and I.M. Govil Nucl Phys. 69, 153, 1965.

33. A. Pasquarelli Nucl. Phys. A93, 218, 1967.

34. N. Ranakumar, E. Kondaiah and R. W. Fink Nucl. Phys. A122, 679, 1968.

35. Jag J. Singh NASA TN D-5946, 1970.

36. G. Andersson - Lindström Zeit für Naturforsch 17a, 238, 1962.

37. S. M. Grimes Nucl. Phys. A124, 369, 1969.

38. A. Rubbino and D. Zubke Nucl. Phys. 85, 606, 1966.

39. E. H. Auerbach ABACUS-2 (Revised Version) BNL-6562, 1962.

40. F. D. Becchetti Jr., and G.W. Greenlees Phys. Rev. 182, 1190, 1969.

41. D. A. Lind and R. B. Day Ann. Phys (N.Y.) 12, 485, 1961.

42. S. C. Mathur, W. E. Tucker, R. W. Benjamin and I. L. Morgan Nucl. Phys. 73, 561, 1965.

43. G. A. Petitt, S. G. Buccino, C. E. Hollandsworth and P. R. Bevington Nucl. Phys. 79, 231, 1966.

44. K. Tsukada et al. Proc. IAEA Cof. on Physics of Fast and Intermediate Reactors (Vienna) Vol I, p 75, 1961.

45. M. A. Rothman, H. S. Hans and C. E. Mandeville Phys. Rev. 100, 83, 1955.

46. H. H. Knitter and M. Coppola Z. Physik 207, 56, 1967.

47. A. R. Sattler et al. Bull Amer. Phys. Soc. 11, 909, 1966.

48. I. L. Morgan et al. USAEC Report TID-20658, Texas Nuclear Corp. Austin, Texas, 1963.

49. D. M. Drake, J. C. Hopkins, C. S. Young, H. Conde and A. Sattler Nucl. Phys. A128, 209, 1969.

50. W. E. Kinney and F. G. Perey ORNL-4517, 1970.

51. J. Martin, D. T. Stewart and W. M. Currie, Nucl. Phys. A113, 564, 1968.

52. F. G. Perey, W. E. Kinney and R.L. Macklin Proc. of Third Conf. on Neutron Cross Sections and Technology Vol. 1, p 191, 1971.

53. U. Fasoli, D. Toniolo and G. Zago INFN/BE-65/5, Padua, Italy, 1965.

54. R. O. Lane et al. Ann. Phys (N.Y.) 12, 135, 1961.

55. M. Coppola and H. H. Knitter EUR-2798e, Geel, 1966.

56. S. Tanaka J. Phys. Soc. Japan 19, 2249, 1964.

57. R. F. Berland CHAD (NAA-SR-11231), Atomics International, Dec. 1965.

58. R. R. Kinsey DUMMY5 Private Communication, 1972.

59. G. B. Beard and G. E. Thomas Nucl. Phys. A157, 520, 1970.

60. V. J. Orphan et al. DASA-2570, GA-10248, 1970.

61. W. E. Tucker, P. S. Buchanan, T. C. Martin D. O. Nellis and G. H. Williams, DASA-2333, July 1969.

62. D. M. Drake, J. C. Hopkins, C. S. Young and H. Conde' Nucl. Sci. & Eng. 40, 294, 1970.

63. J. Gilat GRØGI2, BNL-50246 (T-580), 1970 and H. Takahashi GRØGI-III Private Communication, 1972.

64. A. Gilbert and A. G. W. Cameron, Can. Jour. Phys. 43, 1446, 1965.

65. J. Gilat Phys. Rev. C1, 1432, 1970.

66. J. R. Glover and J. Gilat Phys. Rev. 157, 802, 1967.

67. J. H. Mattauch, W. Thiele and A. H. Wapstra Nucl. Phys. 67, 32, 1965.

68. J. R. Huizenga and G. Igo Nucl. Phys. 29, 462, 1962.

TABLE 1

Properties of the Naturally Occurring Silicon Isotopes

Isotope	Fractional Abundance	Isotopic Mass
^{28}Si	0.9221	27.9769286
^{29}Si	0.0470	28.9764969
^{30}Si	0.0309	29.9737722

TABLE 2

Reaction Q Values for the Silicon Isotopes

Reaction	Q Value (MeV)		
	^{28}Si	^{29}Si	^{30}Si
(n,γ)	8.4738	10.6098	6.5884
(n,p)	- 3.8598	- 2.8980	- 7.7574
(n,np)	-11.5853	-12.3337	-13.507
(n,d)	- 9.3607	-10.1091	-11.2824
(n,t)	-16.1610	-11.5769	-14.4612
(n,^{3}He)	-12.1377	-14.1686	-16.2743
(n,α)	- 2.6529	- 0.0331	- 4.1998
(n,nα)	- 9.9848	-11.1268	-10.6428
(n,2n)	-17.1774	- 8.4738	-10.6097

TABLE 3

Gamma Rays from (n,n'γ) Reactions in ^{28}Si

Initial State		Final State			
Energy (MeV)	J^{π}	Energy (MeV)	J^{π}	E_{γ} (MeV)	Transition Probability (%)
8.941	2^+	1.779	2^+	7.162	50.0
8.941	2^+	0.0	0^+	8.941	50.0
8.902	1^-	1.779	2^+	7.123	100.0
8.588	3^+	6.878	3^-	1.710	10.0
8.588	3^+	6.276	3^+	2.312	10.0
8.588	3^+	1.779	2^+	6.809	80.0
8.543	6^+	4.617	4^+	3.926	100.0
8.413	4^-	6.878	3^-	1.535	86.0
8.413	4^-	6.276	3^+	2.137	2.0
8.413	4^-	4.617	4^+	3.796	4.0
8.413	4^-	1.779	2^+	6.634	8.0
8.328	1^+	1.779	2^+	6.549	45.0
8.328	1^+	0.0	0^+	8.328	55.0
8.260	1^-	1.779	2^+	6.481	80.0
8.260	1^-	0.0	0^+	8.260	20.0
7.935	2^+	1.779	2^+	6.156	20.0
7.935	2^+	0.0	0^+	7.935	80.0
7.798	3^+	6.276	3^+	1.522	25.0
7.798	3^+	1.779	2^+	6.019	75.0
7.416	2^+	1.779	2^+	5.637	10.0
7.416	2^+	0.0	0^+	7.416	90.0
7.381	1^+	1.779	2^+	5.602	55.0
7.381	1^+	0.0	0^+	7.381	45.0
6.889	4^+	1.779	2^+	5.11	100.0
6.878	3^-	1.779	2^+	5.099	30.0
6.878	3^-	0.0	0^+	6.878	70.0
6.691	0^+	1.779	2^+	4.912	100.0
6.276	3^+	4.617	4^+	1.659	10.0
6.276	3^+	1.779	2^+	4.497	90.0
4.975	0^+	1.779	2^+	3.196	100.0
4.617	4^+	1.779	2^+	2.838	100.0
1.779	2^+	0.0	0^+	1.779	100.0

TABLE 4

Gamma Rays from (n,n'γ) Reactions in ^{29}Si

Initial State		Final State		E_γ (MeV)	Transition Probability %
Energy (MeV)	J^π	Energy (MeV)	J^π		
6.379	$1/2^-$	2.425	$3/2^+$	3.954	8.0
6.379	$1/2^-$	1.273	$3/2^+$	5.106	22.0
6.379	$1/2^-$	0.0	$1/2^+$	6.379	70.0
4.933	$3/2^-$	1.273	$3/2^+$	3.660	8.0
4.933	$3/2^-$	0.0	$1/2^+$	4.933	92.0
3.623	$7/2^-$	3.067	$5/2^+$	0.556	9.0
3.623	$7/2^-$	2.028	$5/2^+$	1.595	90.0
3.623	$7/2^-$	1.273	$3/2^+$	2.350	1.0
3.067	$5/2^+$	2.028	$5/2^+$	1.039	22.0
3.067	$5/2^+$	1.273	$3/2^+$	1.794	78.0
2.425	$3/2^+$	1.273	$3/2^+$	1.152	12.0
2.425	$3/2^+$	0.0	$1/2^+$	2.425	88.0
2.028	$5/2^+$	1.273	$3/2^+$	0.755	5.0
2.028	$5/2^+$	0.0	$1/2^+$	2.028	95.0
1.273	$3/2^+$	0.0	$1/2^+$	1.273	100.0

TABLE 5

Gamma Rays from (n,n'γ) Reactions in ^{30}Si

Initial State		Final State		E_γ	Transition Probability %
Energy (MeV)	J^π	Energy (MeV)	J^π		
6.745	1^-	0.0	0^+	6.745	100.0
5.280	4^+	0.0	0^+	5.280	100.0
4.830	3^+	2.235	2^+	2.595	50.0
4.830	3^+	0.0	0^+	4.830	50.0
4.809	2^+	2.235	2^+	2.574	50.0
4.809	2^+	0.0	0^+	4.809	50.0
3.788	0^+	2.235	2^+	1.553	100.0
3.770	1^+	2.235	2^+	1.535	60.0
3.770	1^+	0.0	0^+	3.770	40.0
3.498	2^+	2.235	2^+	1.263	55.0
3.498	2^+	0.0	0^+	3.498	45.0
2.235	2^+	0.0	0^+	2.235	100.0

TABLE 6

Gamma-Ray Energies and Multiplicities due to Thermal Neutron Capture in Silicon

E_γ (MeV)	I_γ Photons/100 Capture	$E_{initial}$ (MeV)	Target Isotope
10.611	0.3	primary	^{29}Si
8.474	2.7	primary	^{28}Si
8.373	0.1	primary	^{29}Si
7.846	0.15		
7.201	9.0	primary	^{28}Si
7.113	0.2	primary	^{29}Si
7.057	0.1	7.057	^{28}Si
6.746	1.3	6.746	^{29}Si
6.446	0.1	primary	^{28}Si
6.420	0.2		
6.381	13.5	6.3810	^{28}Si
6.047	0.6	primary	^{28}Si
5.272	1.0	7.507	^{29}Si
5.1080	4.1	6.3810	^{28}Si
4.9350	65.0	4.9350	^{28}Si
4.8410	0.25	4.8410	^{28}Si
3.9550	2.0	6.3810	^{28}Si
3.8650	1.4	primary	^{29}Si
3.7700	0.2	3.7700	^{29}Si
3.6620	3.7	4.9340	^{28}Si
3.5390	69.0	primary	^{28}Si
3.1020	1.2	primary	^{29}Si
3.054	1.4	primary	^{30}Si
2.7820	1.6	3.5330	^{30}Si
2.4460	0.3		
2.4260	2.8	2.4260	^{28}Si
2.2350	1.8	2.235	^{29}Si
2.2050	0.2	primary	^{30}Si
2.093	2.1	primary	^{28}Si
2.0280	0.5	2.0280	^{28}Si
1.8670	0.6	4.934	^{28}Si
1.794	0.6	3.067	^{28}Si
1.695	0.1	1.6950	^{30}Si
1.565	0.4	primary	^{28}Si
1.552	0.3	3.7870	^{29}Si
1.541	0.5	6.3810	^{28}Si
1.535	0.3	3.7700	^{29}Si
1.446	0.7	6.3810	^{28}Si
1.273	19.0	1.273	^{28}Si
1.152	0.5	2.426	^{28}Si
0.752	1.6	0.7520	^{30}Si

TABLE 7

Optical Model Parameters

$$V(r) = - V_R f(r,R_R,a_R) + V_{SO}\, \underline{\sigma} \cdot \underline{\ell}\, \lambda\!\!\!^{-2}_{\pi} \left(\frac{1}{r}\right)\left(\frac{d}{dr}\right)\left[f(r,R_{SO},a_{SO})\right] \quad \text{Real Part}$$

$$W(r) = -W_v\, f(r,R_I',a_I') + W_{SF}\, 4a_I \left(\frac{d}{dr}\right)\left[f(f,R_I,a_I)\right] \quad \text{Imaginary Part}$$

where $f(r,R,a) = \dfrac{1}{1 + e^{(r-R)/a}}$

$\underline{\sigma} \cdot \underline{\ell}$ = scalar product of intrinsic and orbital angular momentum operators.

$\lambda\!\!\!^{-2}_{\pi}$ = pion Compton wave-length squared $\simeq 2.0 \text{fm}^2$.

A = target mass number.

All radii of the form: $R_I = r_I A^{1/3}$.

$V_R = 56.3 - 0.32E - 24.0 \dfrac{(N-Z)}{A}$

$r_R = 1.17 \quad a_R = 0.75$

$W_v = 0$

$W_{SF} = 13.0 - 0.25E - 12.0 \dfrac{(N-Z)}{A}$ or zero, whichever is greater.

$r_I = r_{I'} = 1.26 \qquad a_I = a_{I'} = 0.58$

$V_{SO} = 6.2 \quad r_{SO} = 1.01 \quad a_{SO} = 0.75$ where E is the incident neutron lab energy in MeV.

TABLE 8

Level Density Parameters of the Isotopes Used in the Cascade Calculations*

	a	T	E_o	E_x	σ	δ
^{29}Si	3.57	1.91	0.75	8.1	2.1	2.09
^{28}Si	3.05	2.09	3.20	12.9	2.0	3.89
^{27}Si	2.6	1.91		8.1	2.0	2.09
^{28}Aℓ	3.65	1.50	-0.70	6.8	2.2	0
^{27}Aℓ	3.45	2.08	-0.35	9.6	2.0	1.80
^{27}Mg	4.0	2.04	-0.80	12.2	2.25	2.46
^{25}Mg	3.85	2.12	-1.00	12.4	2.15	2.46
^{24}Mg	3.32	2.18	2.80	13.0	2.0	5.31

*where a = level density parameters (MeV^{-1}), T = temperature of nuclei (MeV), E_o = normalization energy (MeV), E_x = energy of tangency point (MeV), σ = spin cut-off parameter; δ = pairing energy (MeV).

TABLE 9

Yrast Levels of Nuclei Produced by Cascade Processes in ^{28}Si Neutron Reactions

Spin	^{29}Si	^{28}Si	^{27}Si	^{28}Al	^{27}Al	^{27}Mg	^{25}Mg	^{24}Mg	^{24}Na	^{21}Ne
0 or 1/2	0.	0.0	0.780	6.0	0.842	0.0	0.5852	0.0	0.5633	2.4
1	1.273	7.382	0.953	1.372	1.013	0.984	0.9747	7.561	3.37	0.0
2	2.0	1.778	0.0	0.030	0.	1.692	0.	1.368	0.0	0.347
3	3.623	6.690	2.165	0.0	2.209	3.757	1.6137	5.228	3.8	1.75
4	5.472	4.614	5.472	2.207	3.000	5.757	3.400	4.122	3.22	4.122
5	7.143	8.897	7.143	2.49	7.287	7.633	7.633	8.864	7.633	8.864
6	9.147	11.10	9.147	6.025	9.464	9.685	9.685	12.462	9.685	12.462
7	11.486	13.704	11.486	8.201	12.003	12.078	12.078	15.109	12.078	15.164
8	14.158	16.708	14.158	10.711	14.905	14.814	14.814	18.164	14.814	18.164
9	17.165	20.113	17.165	13.556	18.170	17.892	17.892	21.626	17.892	21.626
10	20.505	23.50	20.505	16.736	21.798	21.312	21.312	25.3	21.312	25.3
11	24.18	27.18	24.18	20.251	25.25	25.074	25.074	29.0	25.07	29.0
12	28.19	31.19	28.19	24.10	29.10	29.10	29.178	33.17	29.18	33.17

TABLE 10

Binding Energies of Neutron, Proton, and α-Particles for Nuclei Produced by Cascade Processes in ^{28}Si Neutron Reactions (MeV)

	^{29}Si		^{28}Si		^{27}Si		^{28}Al		^{27}Al	
n	^{28}Si	8.475	^{27}Si	17.175	^{26}Si	13.32	^{27}Al	7.731	^{26}Al	13.057
p	^{28}Al	12.327	^{27}Al	11.583	^{26}Al	7.464	^{27}Mg	9.562	^{26}Mg	8.271
α	^{25}Mg	11.128	^{24}Mg	9.981	^{23}Mg	9.338	^{24}Na	10.862	^{23}Na	10.093

	^{25}Mg		^{24}Mg		^{24}Na		$^{21}Ne^*$	
n	^{24}Mg	7.329	^{23}Mg	16.532	^{23}Na	6.961	^{20}Ne	6.759
p	^{24}Na	12.061	^{23}Na	11.694	^{23}Na	10.599	^{20}F	13.007
α	^{21}Ne	9.886	^{20}Ne	9.317	^{20}Fe	10.83	^{17}O	7.347

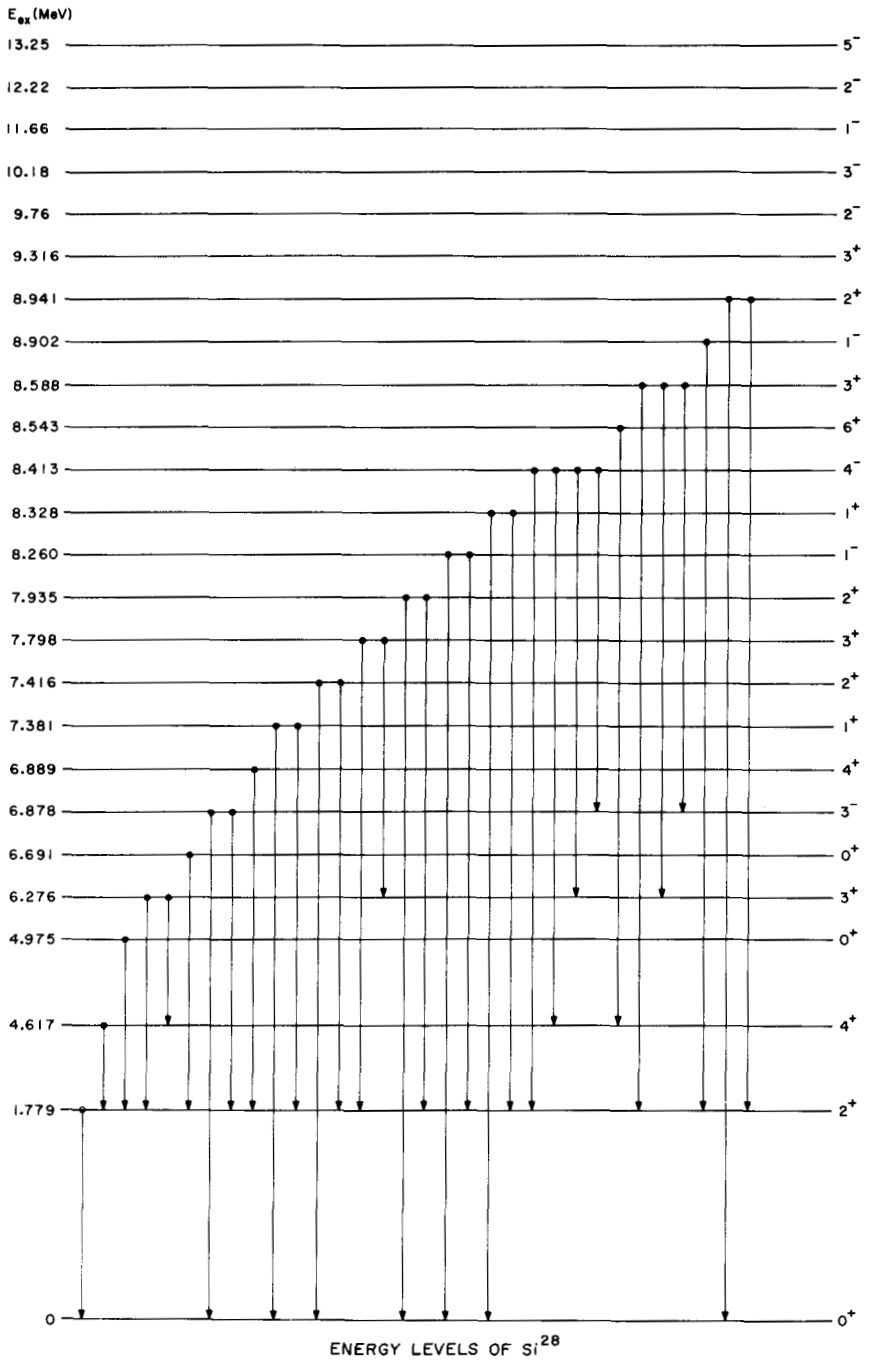

ENERGY LEVELS OF Si^{28}

Figure 1

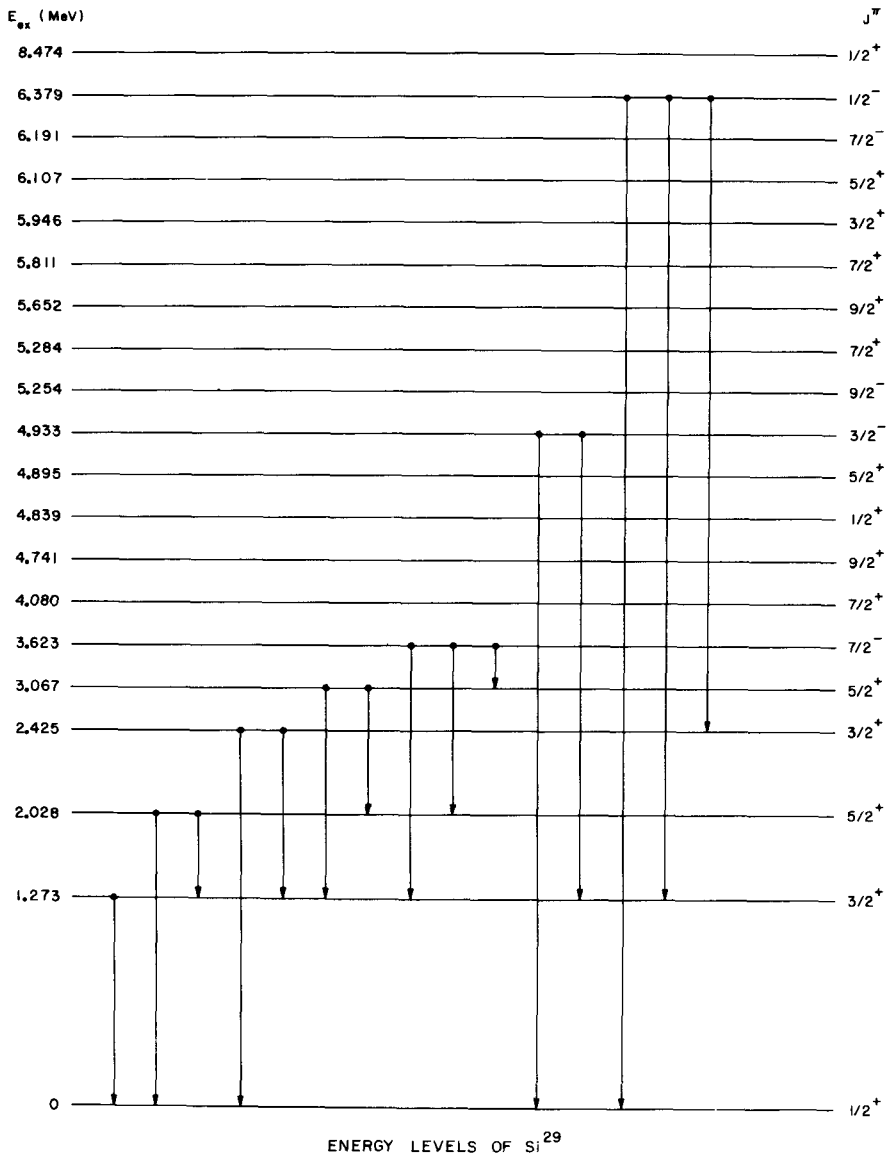

ENERGY LEVELS OF Si^{29}

Figure 2

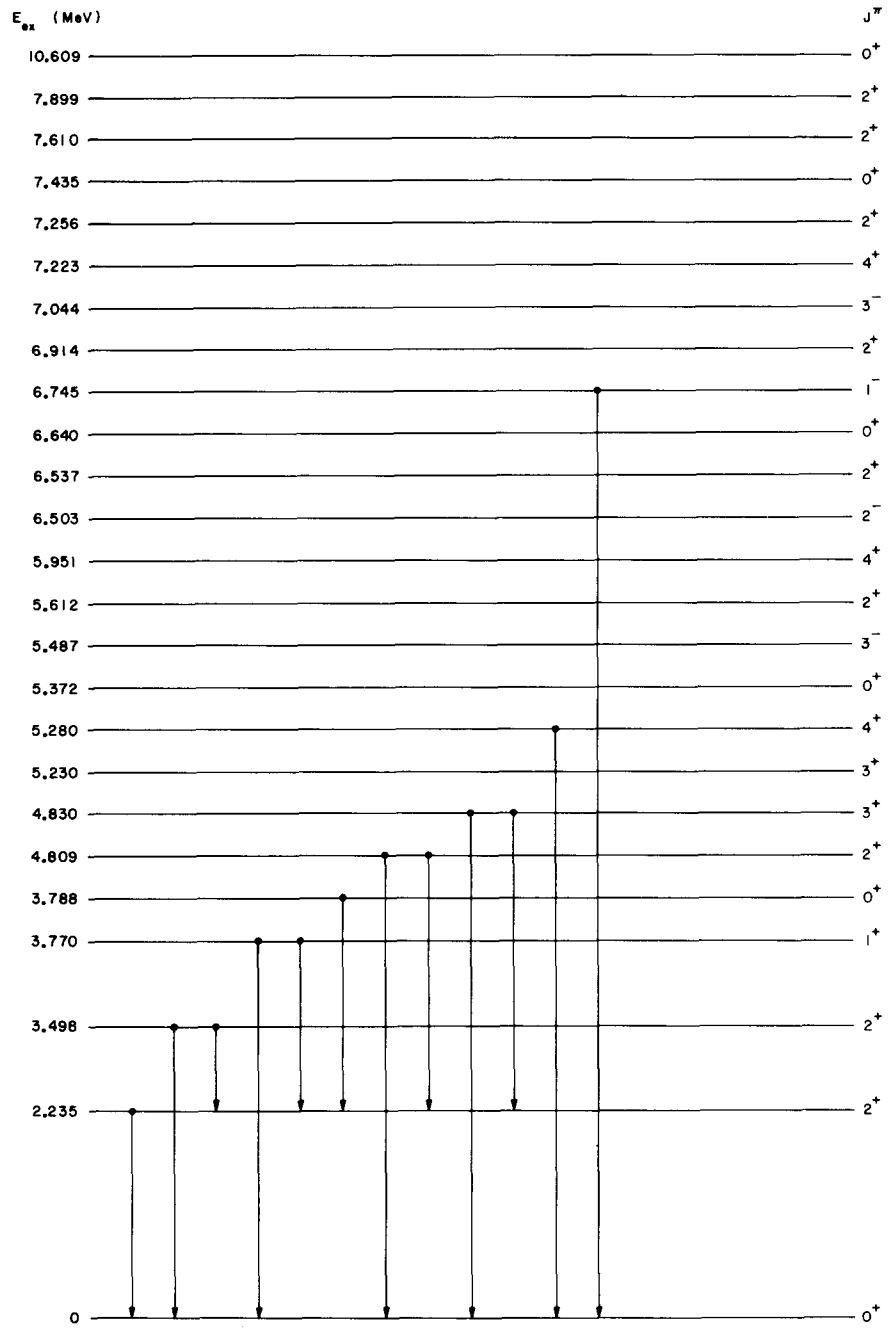

ENERGY LEVELS OF Si^{30}

Figure 3

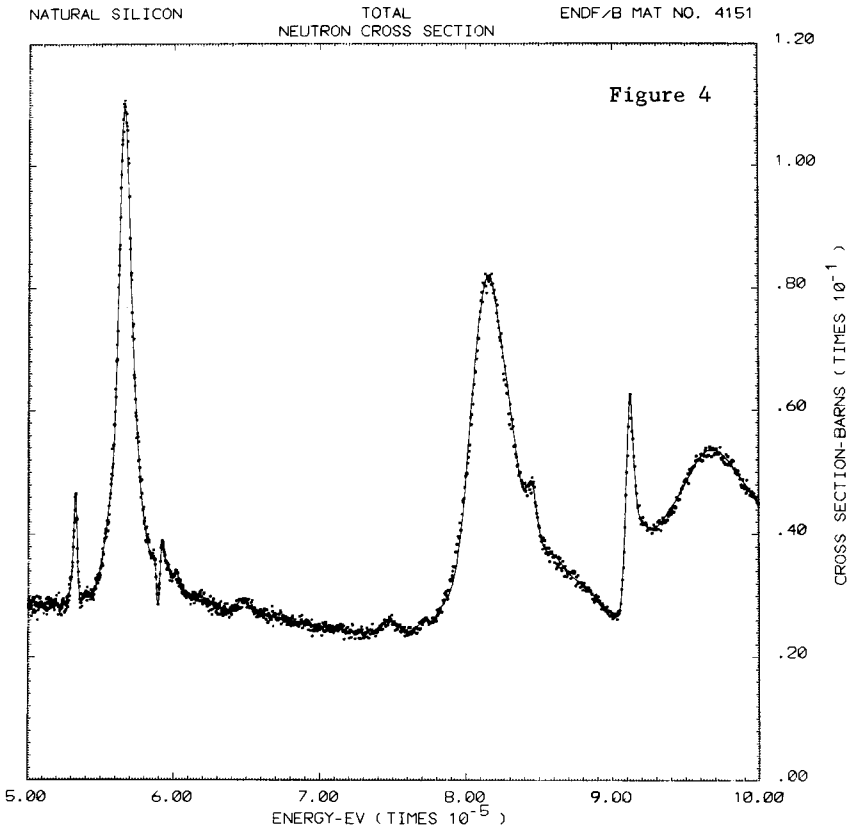
NATURAL SILICON
TOTAL
NEUTRON CROSS SECTION
ENDF/B MAT NO. 4151
Figure 4
1.20
1.00
.80
.60
.40
.20
.00
CROSS SECTION-BARNS (TIMES 10^{-1})
5.00
6.00
7.00
8.00
9.00
10.00
ENERGY-EV (TIMES 10^{-5})

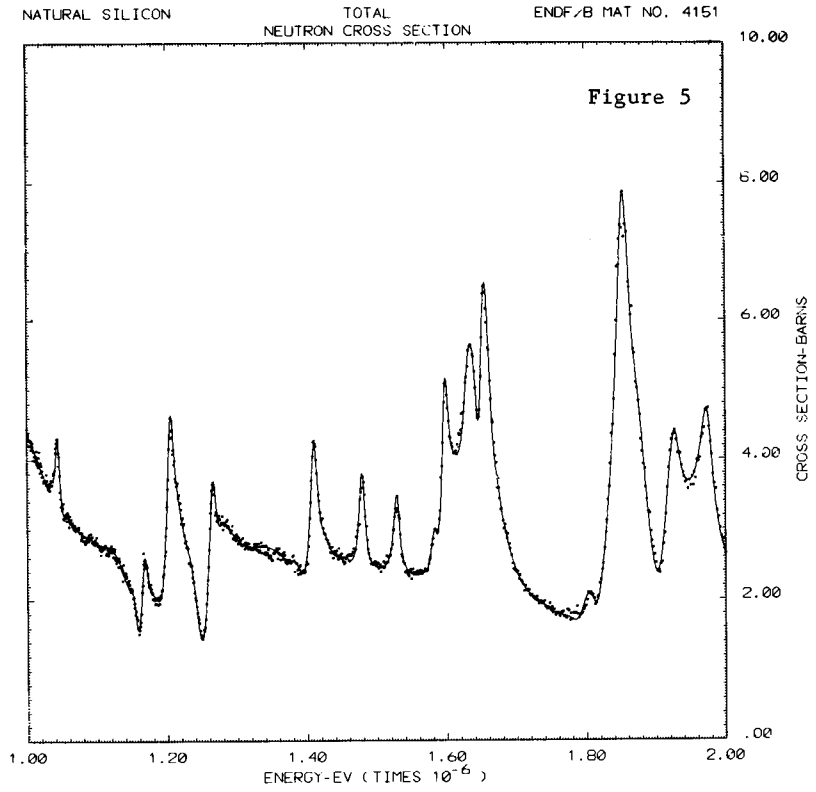
NATURAL SILICON
TOTAL
NEUTRON CROSS SECTION
ENDF/B MAT NO. 4151
Figure 5
10.00
8.00
6.00
4.00
2.00
.00
CROSS SECTION-BARNS
1.00
1.20
1.40
1.60
1.80
2.00
ENERGY-EV (TIMES 10^{-6})

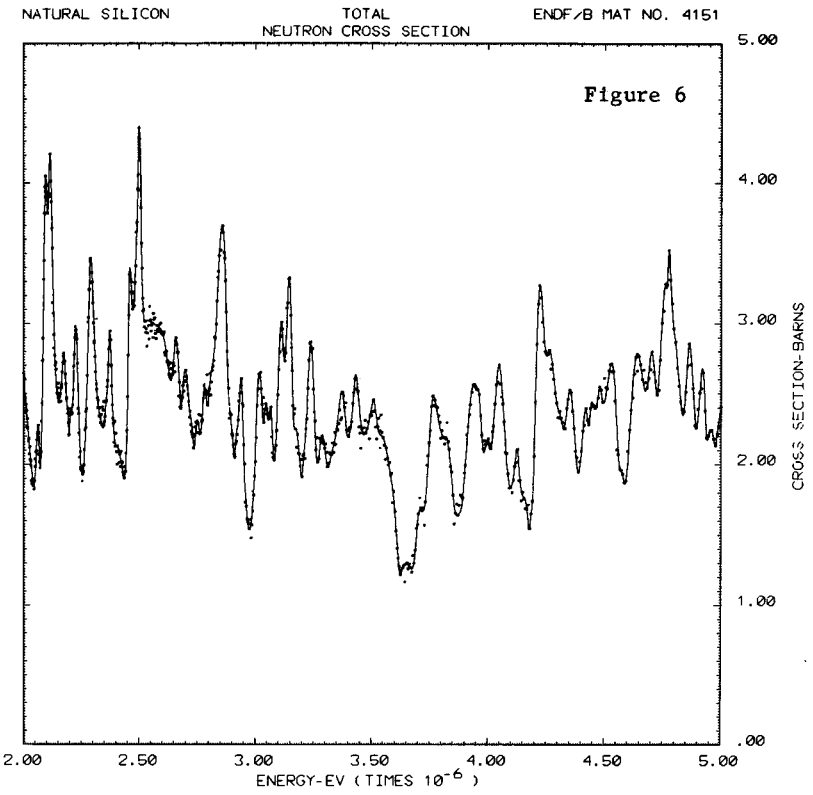
NATURAL SILICON
TOTAL
NEUTRON CROSS SECTION
ENDF/B MAT NO. 4151
Figure 6
5.00
4.00
3.00
2.00
1.00
.00
CROSS SECTION-BARNS
2.00
2.50
3.00
3.50
4.00
4.50
5.00
ENERGY-EV (TIMES 10-6)

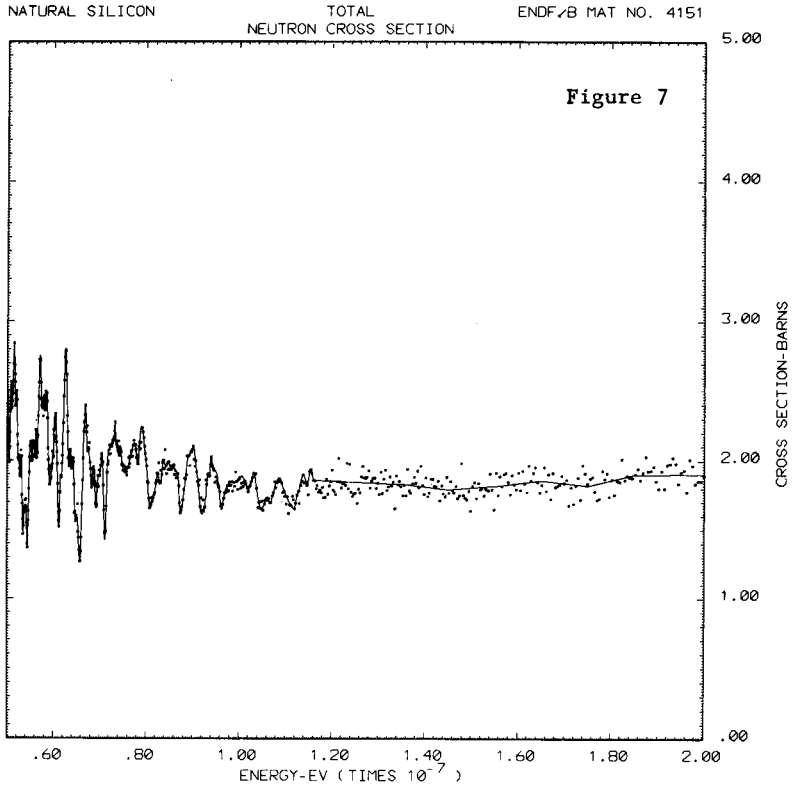
NATURAL SILICON
TOTAL
NEUTRON CROSS SECTION
ENDF/B MAT NO. 4151
Figure 7
5.00
4.00
3.00
2.00
1.00
.00
CROSS SECTION-BARNS
.60
.80
1.00
1.20
1.40
1.60
1.80
2.00
ENERGY-EV (TIMES 10-7)

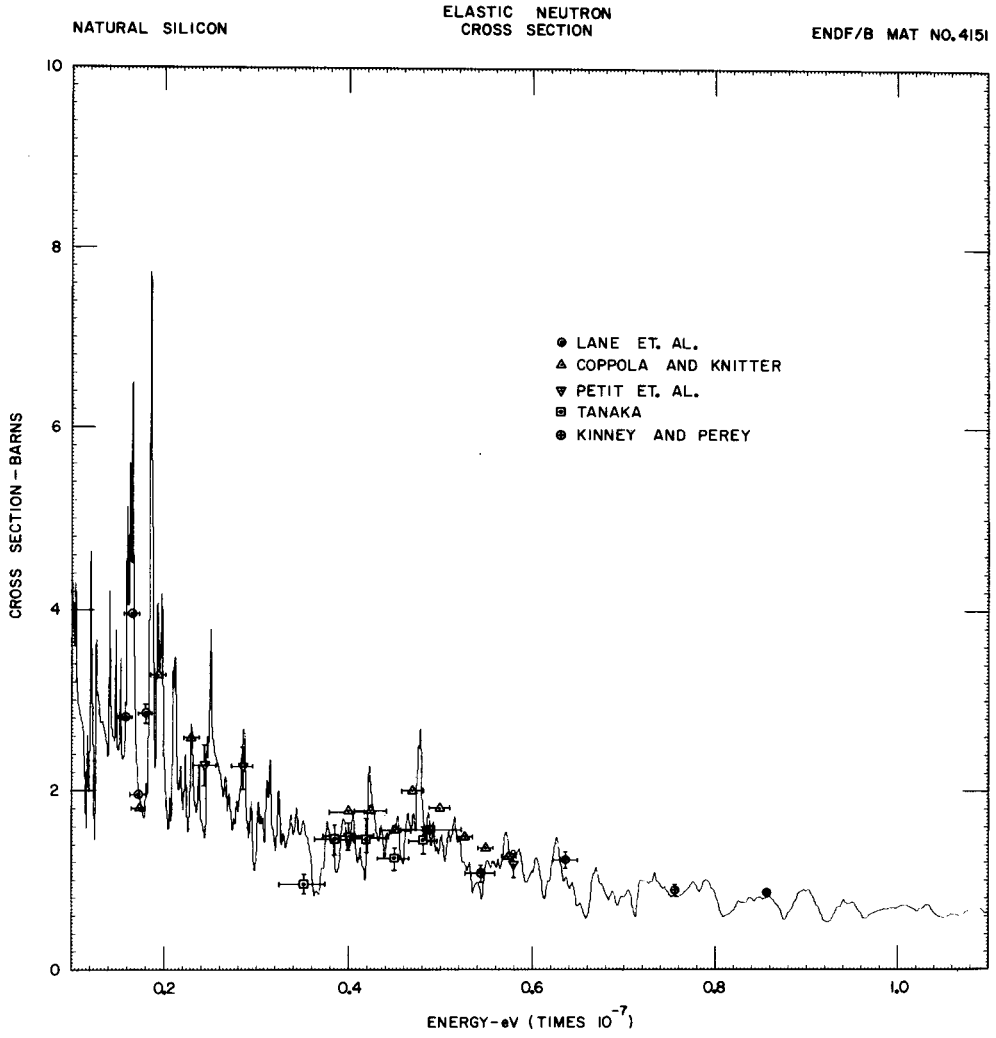
NATURAL SILICON
ELASTIC NEUTRON
CROSS SECTION
ENDF/B MAT NO. 4151
CROSS SECTION - BARNS
ENERGY - eV (TIMES 10^{-7})
LANE ET. AL.
COPPOLA AND KNITTER
PETIT ET. AL.
TANAKA
KINNEY AND PEREY
0
2
4
6
8
10
0.2
0.4
0.6
0.8
1.0

Figure 8

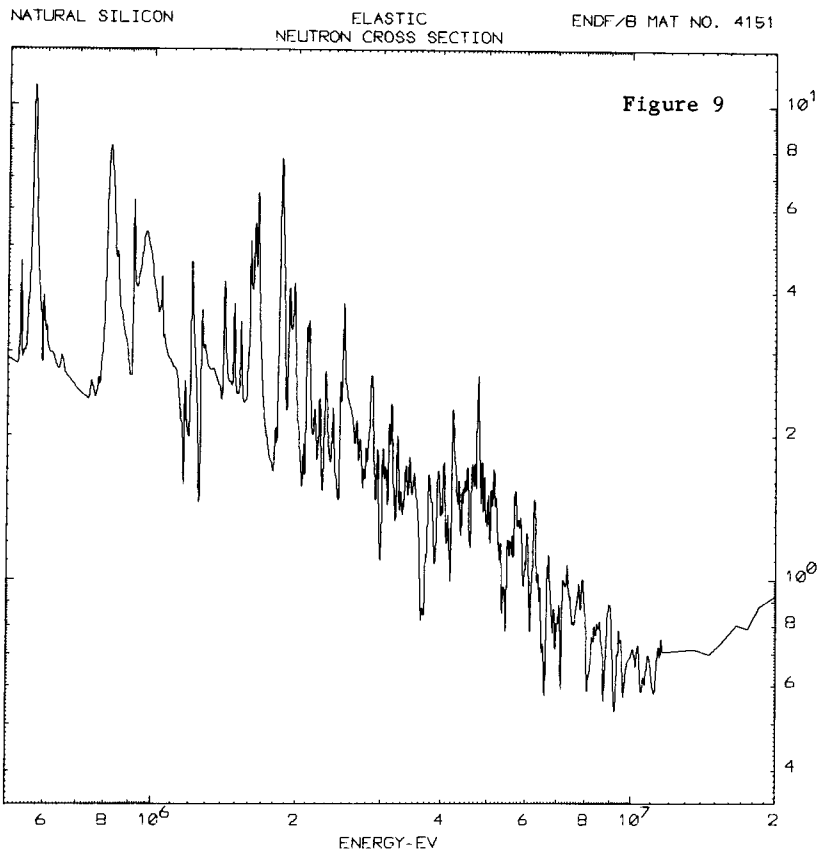
NATURAL SILICON
ELASTIC
NEUTRON CROSS SECTION
ENDF/B MAT NO. 4151
Figure 9
10^1
8
6
4
2
10^0
8
6
4
6
8
10^6
2
4
6
8
10^7
2
ENERGY-EV

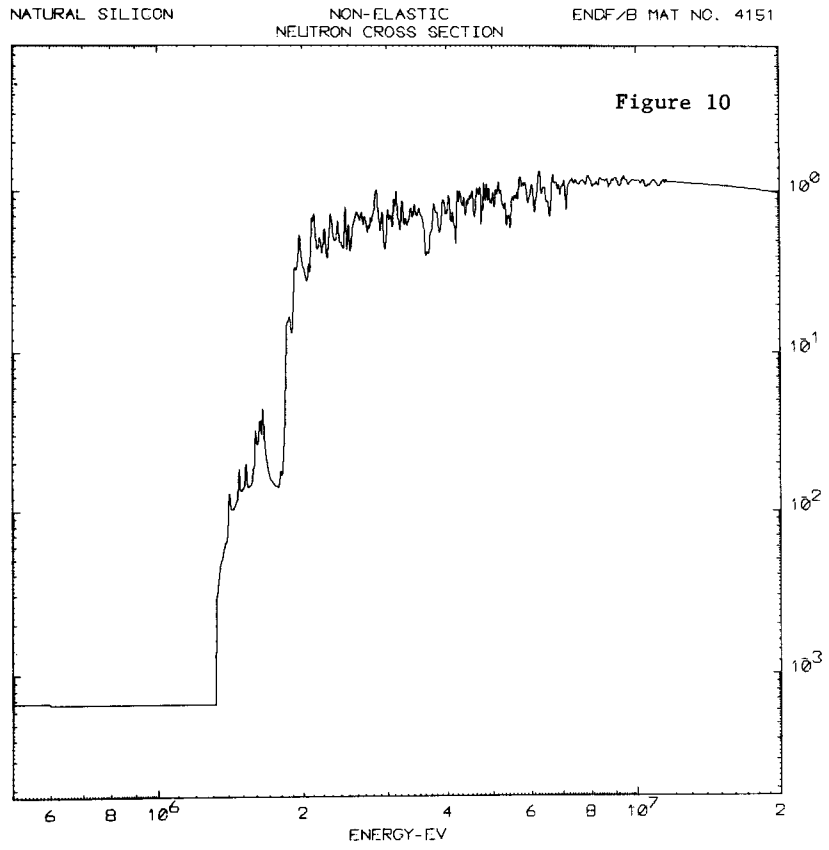
NATURAL SILICON
NON-ELASTIC
NEUTRON CROSS SECTION
ENDF/B MAT NO. 4151
Figure 10
10^0
10^1
10^2
10^3
6
8
10^6
2
4
6
8
10^7
2
ENERGY-EV

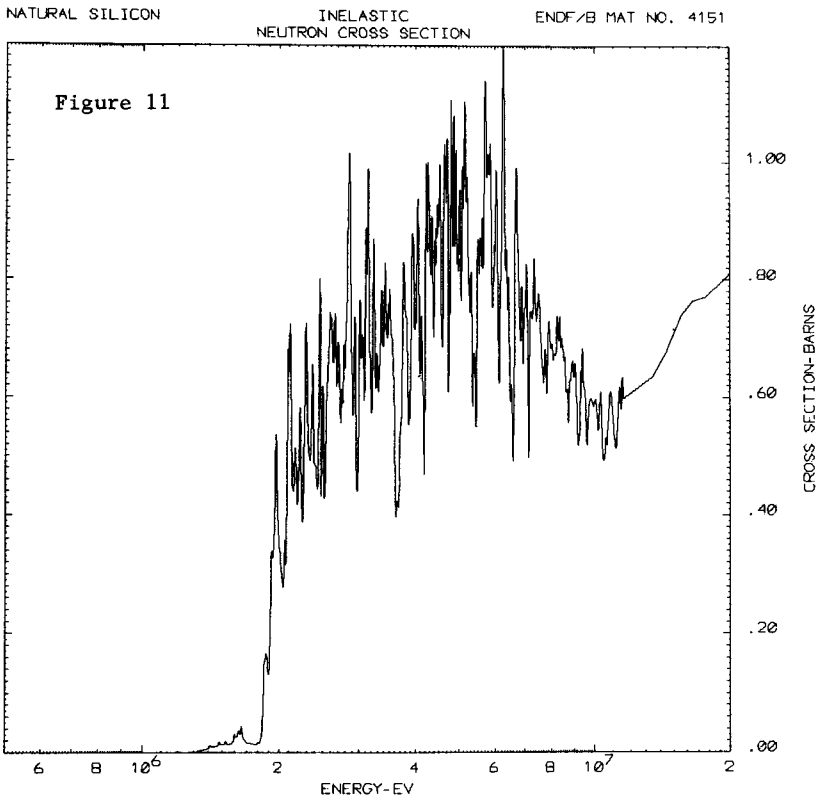

Figure 11

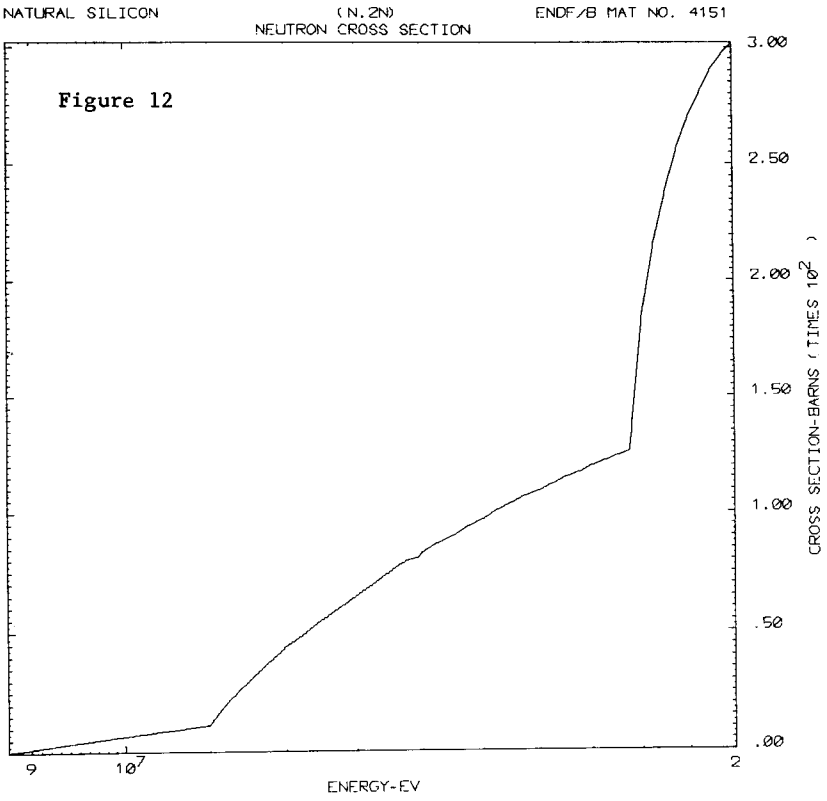

Figure 12

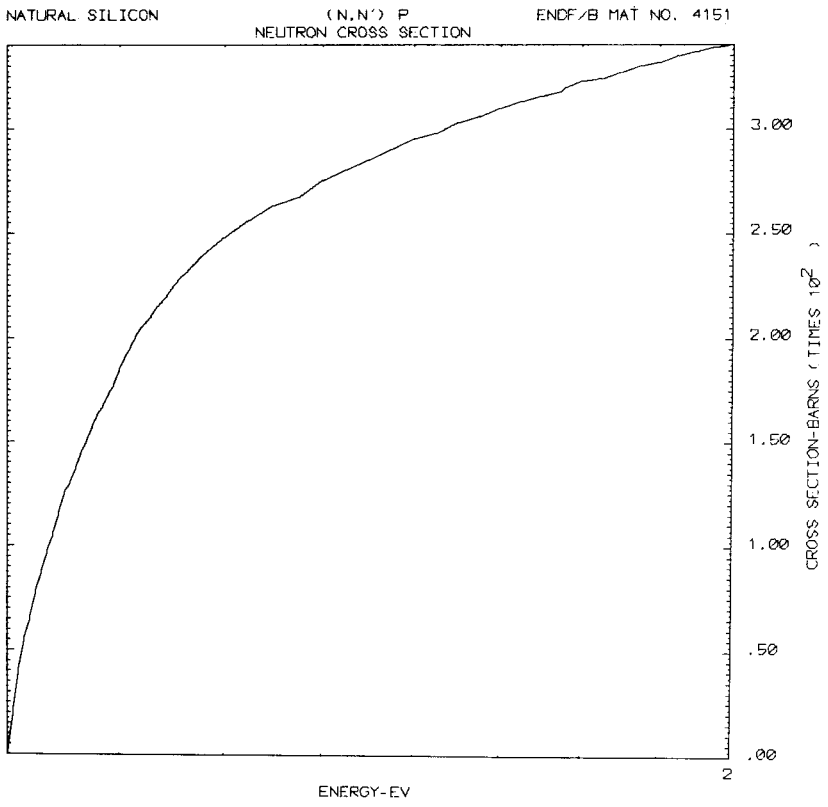
NATURAL SILICON
(N,N') P
NEUTRON CROSS SECTION
ENDF/B MAT NO. 4151
3.00
2.50
2.00
1.50
1.00
.50
.00
CROSS SECTION-BARNS (TIMES 10^2)
2
ENERGY-EV

Figure 13

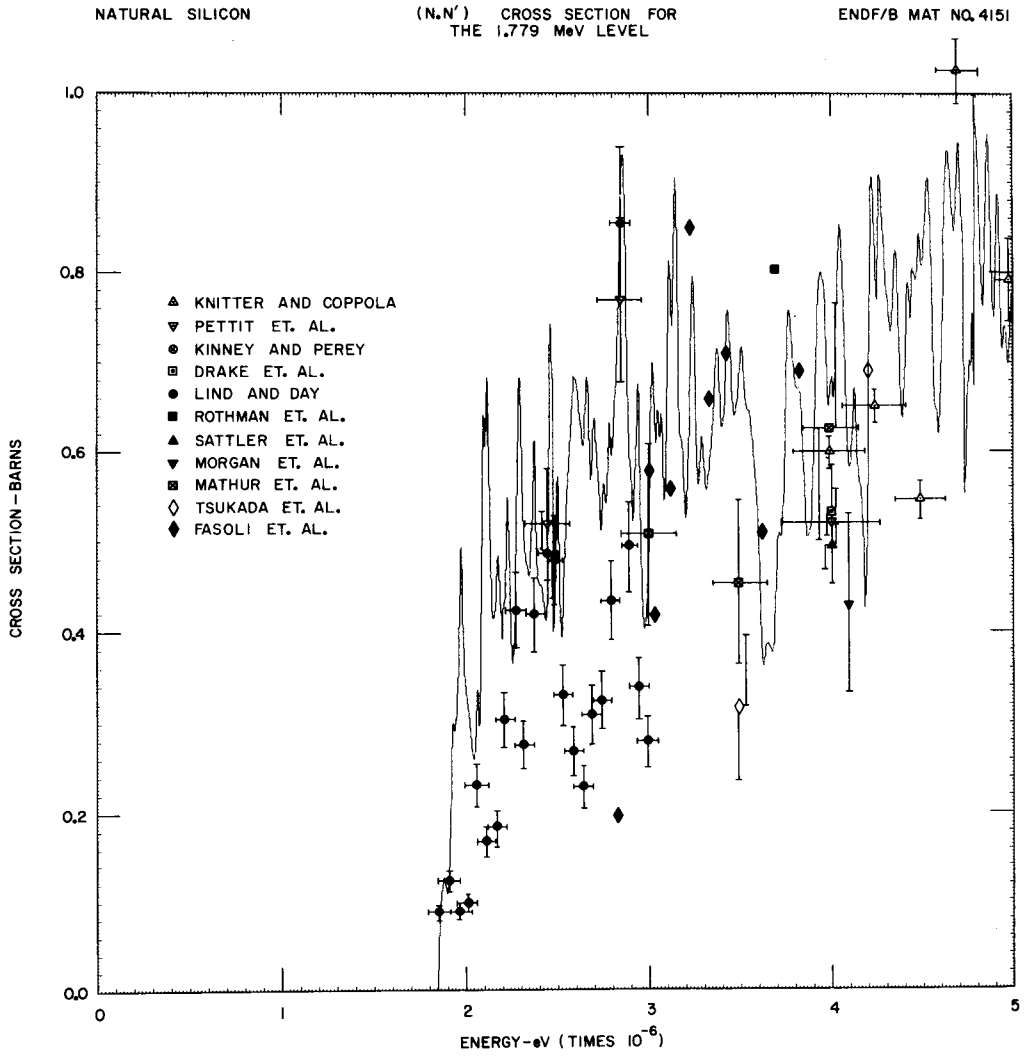
NATURAL SILICON
(N,N') CROSS SECTION FOR THE 1.779 MeV LEVEL
ENDF/B MAT NO. 4151
KNITTER AND COPPOLA
PETTIT ET. AL.
KINNEY AND PEREY
DRAKE ET. AL.
LIND AND DAY
ROTHMAN ET. AL.
SATTLER ET. AL.
MORGAN ET. AL.
MATHUR ET. AL.
TSUKADA ET. AL.
FASOLI ET. AL.
CROSS SECTION - BARNS
ENERGY - eV (TIMES 10^-6)
0.0
0.2
0.4
0.6
0.8
1.0
0
1
2
3
4
5

Figure 14

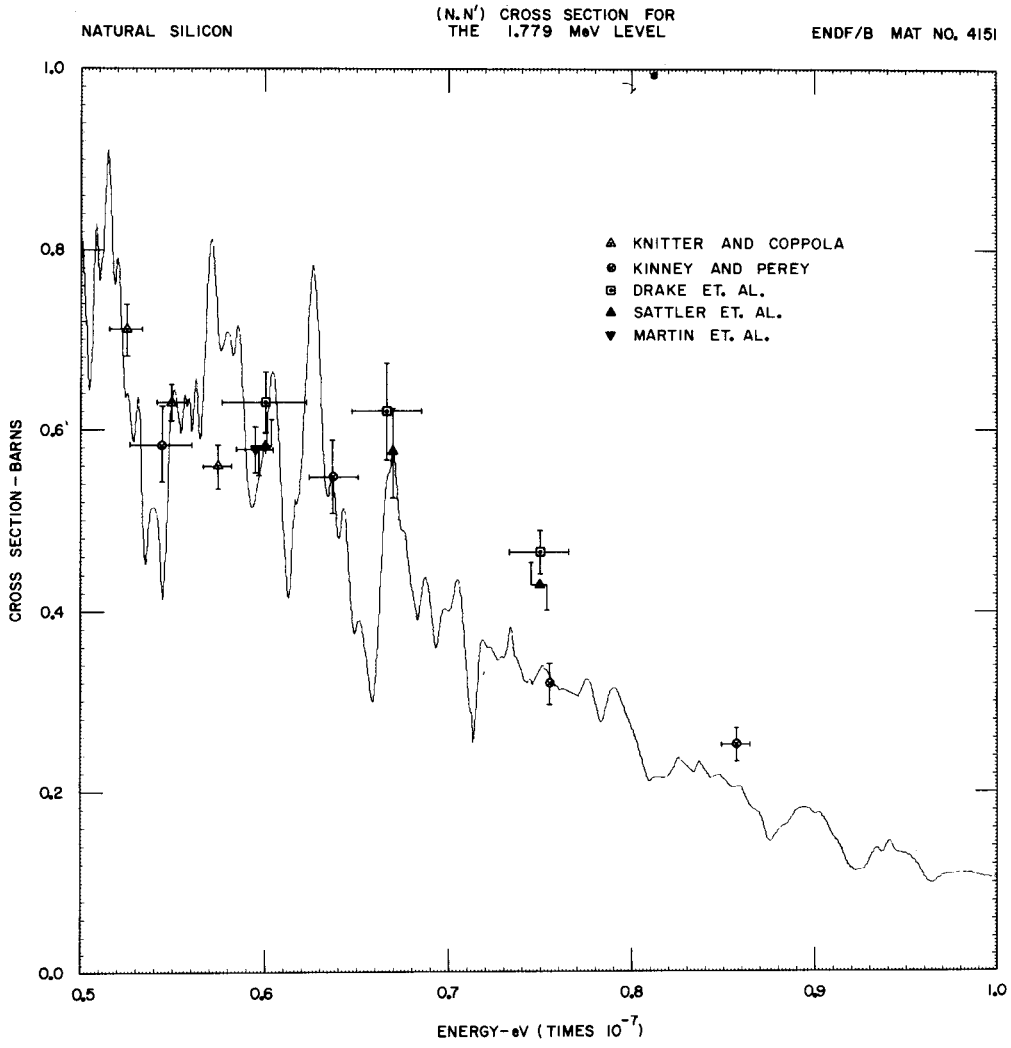
NATURAL SILICON
(N,N') CROSS SECTION FOR THE 1.779 MeV LEVEL
ENDF/B MAT NO. 4151
KNITTER AND COPPOLA
KINNEY AND PEREY
DRAKE ET. AL.
SATTLER ET. AL.
MARTIN ET. AL.
CROSS SECTION - BARNS
ENERGY - eV (TIMES 10^-7)
1.0
0.8
0.6
0.4
0.2
0.0
0.5
0.6
0.7
0.8
0.9
1.0

Figure 15

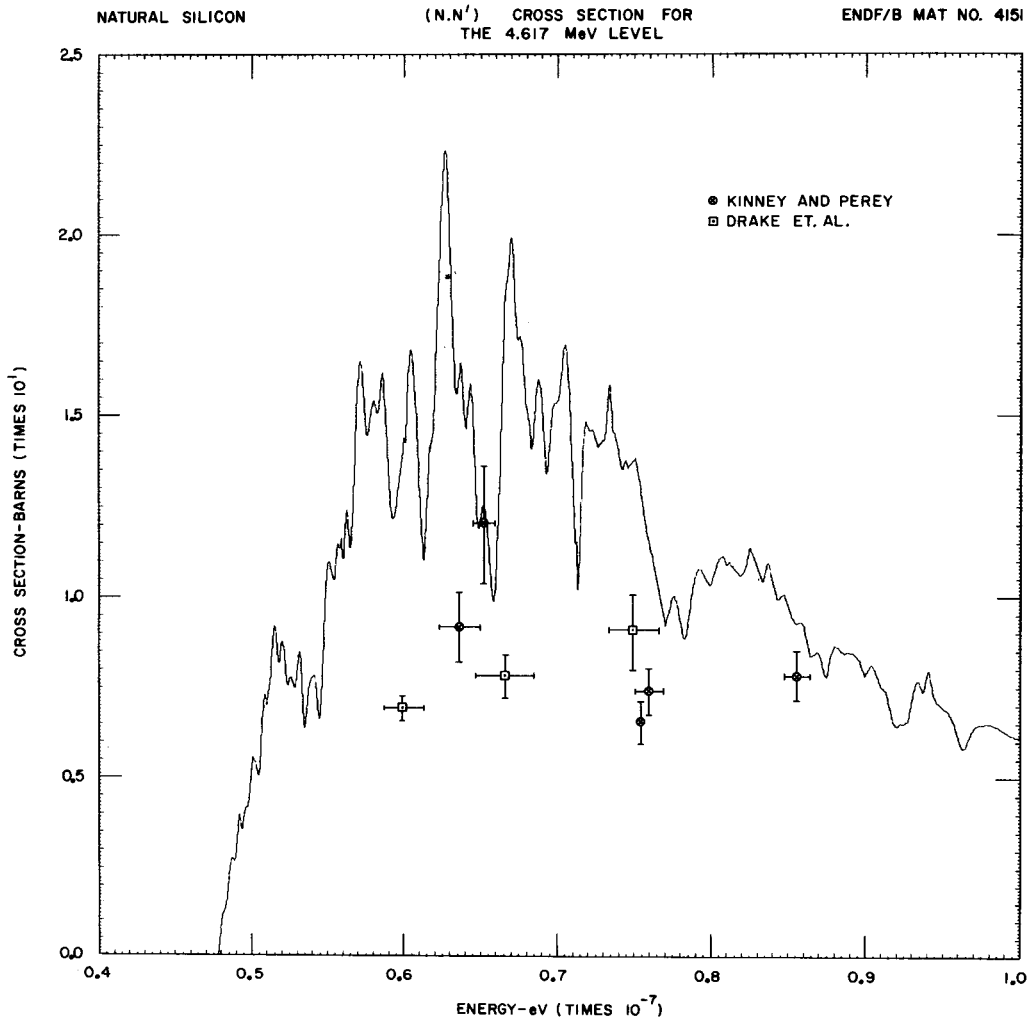
NATURAL SILICON
(N.N') CROSS SECTION FOR THE 4.617 MeV LEVEL
ENDF/B MAT NO. 4151
KINNEY AND PEREY
DRAKE ET. AL.
CROSS SECTION-BARNS (TIMES 10')
ENERGY-eV (TIMES 10^-7)
2.5
2.0
1.5
1.0
0.5
0.0
0.4
0.5
0.6
0.7
0.8
0.9
1.0

Figure 16

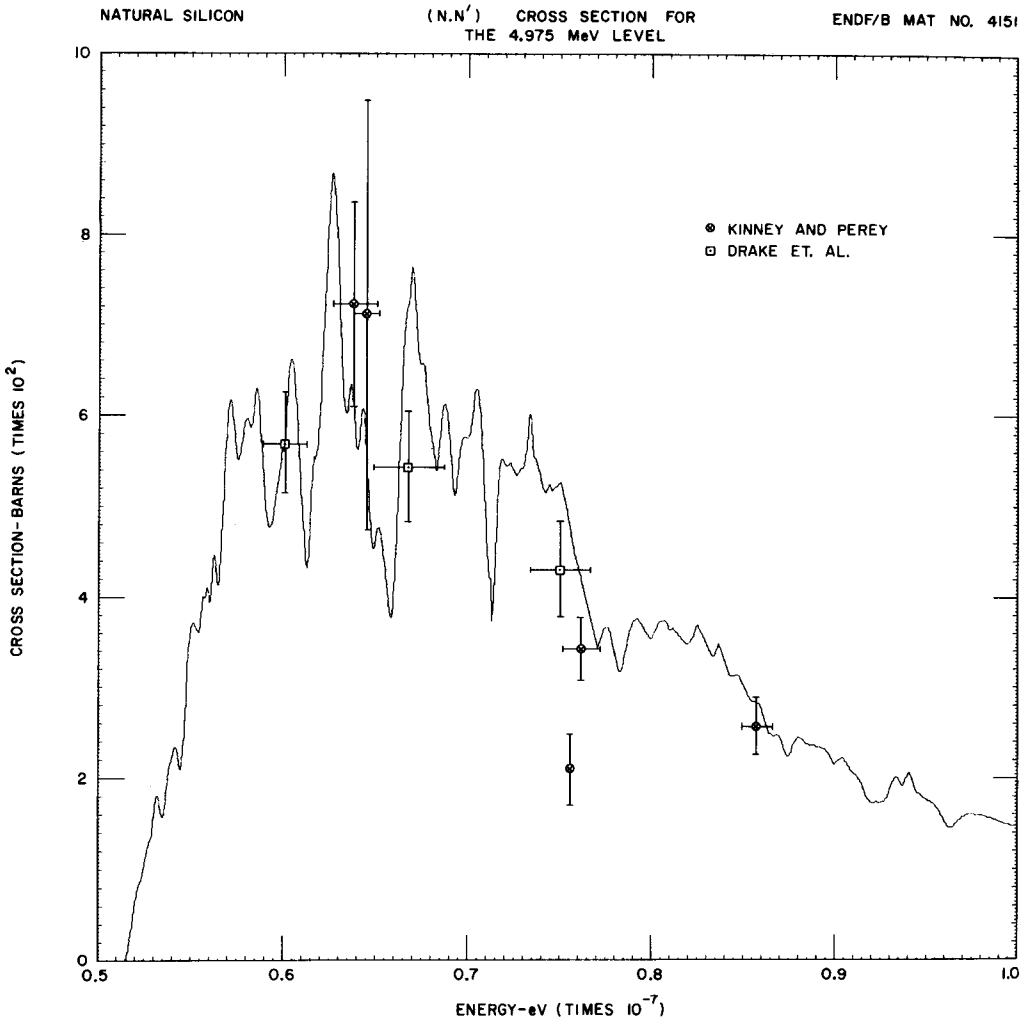
NATURAL SILICON
(N.N′) CROSS SECTION FOR THE 4.975 MeV LEVEL
ENDF/B MAT NO. 4151
KINNEY AND PEREY
DRAKE ET. AL.
CROSS SECTION-BARNS (TIMES 10²)
ENERGY-eV (TIMES 10⁻⁷)
0
2
4
6
8
10
0.5
0.6
0.7
0.8
0.9
1.0

Figure 17

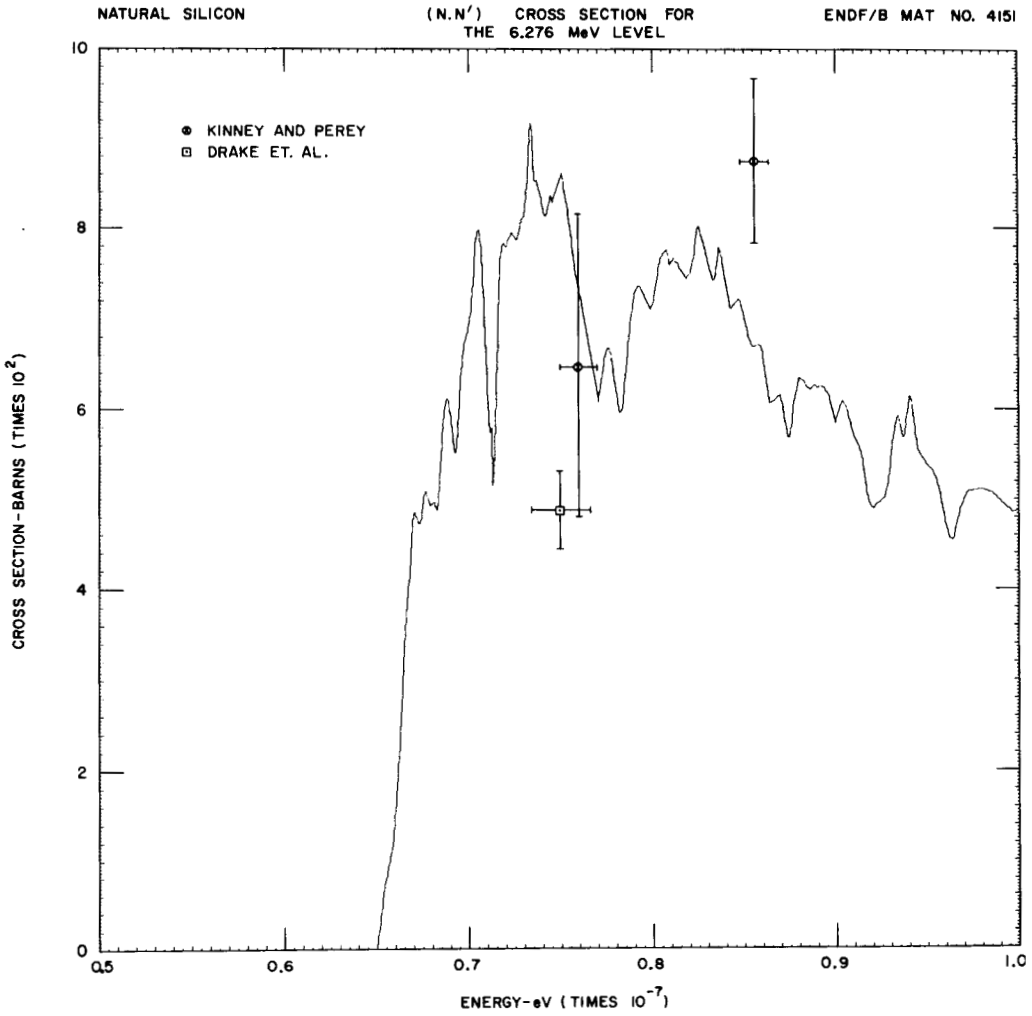
NATURAL SILICON
(N.N') CROSS SECTION FOR THE 6.276 MeV LEVEL
ENDF/B MAT NO. 4151
KINNEY AND PEREY
DRAKE ET. AL.
CROSS SECTION-BARNS (TIMES 10^2)
ENERGY-eV (TIMES 10^-7)
0
2
4
6
8
10
0.5
0.6
0.7
0.8
0.9
1.0

Figure 18

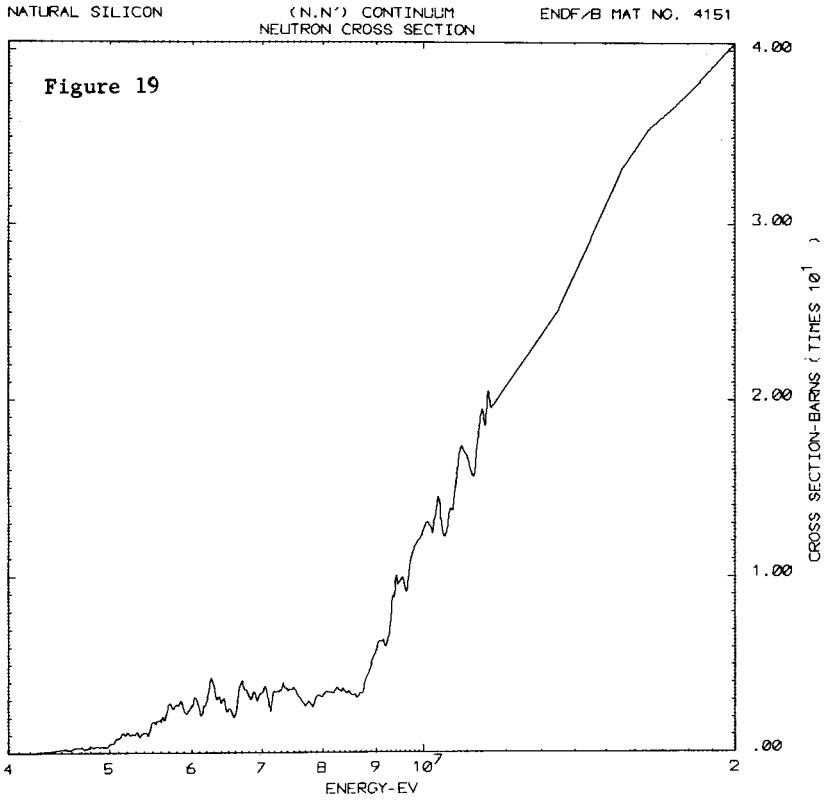

Figure 19

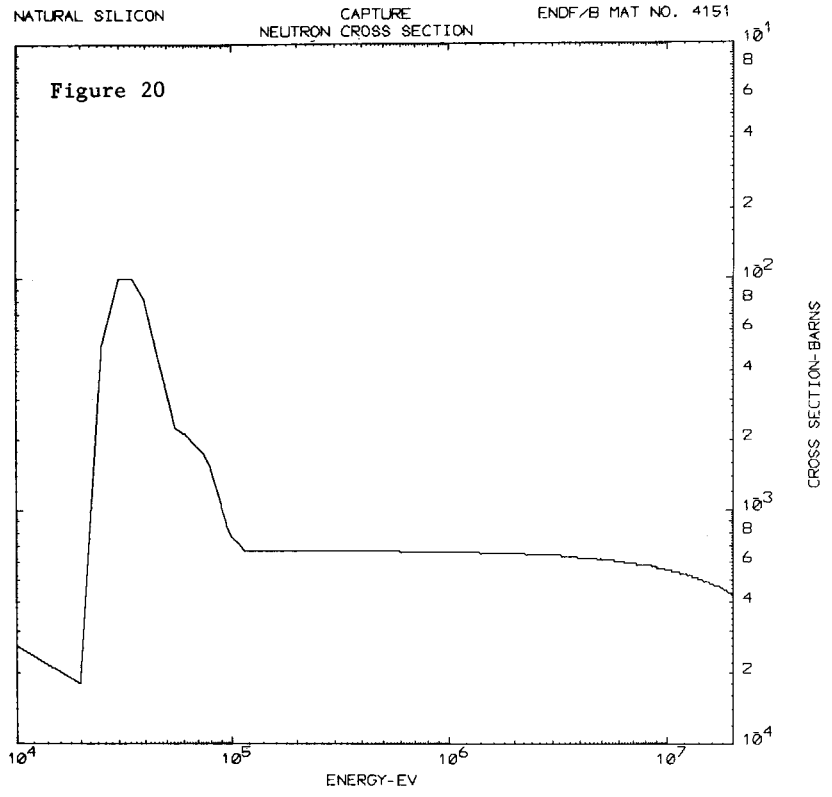

Figure 20

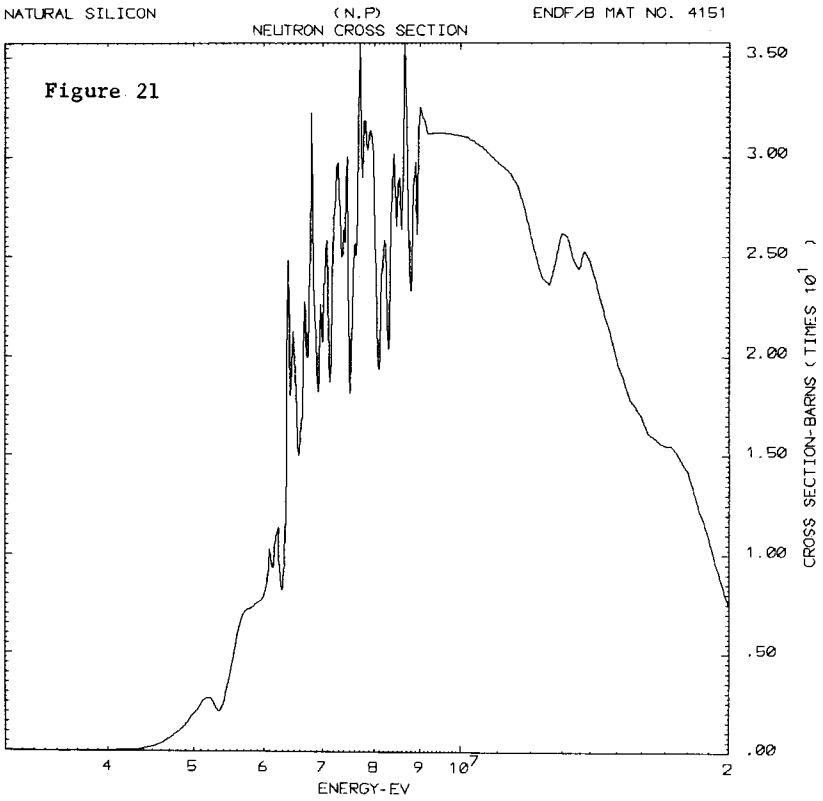

Figure 21

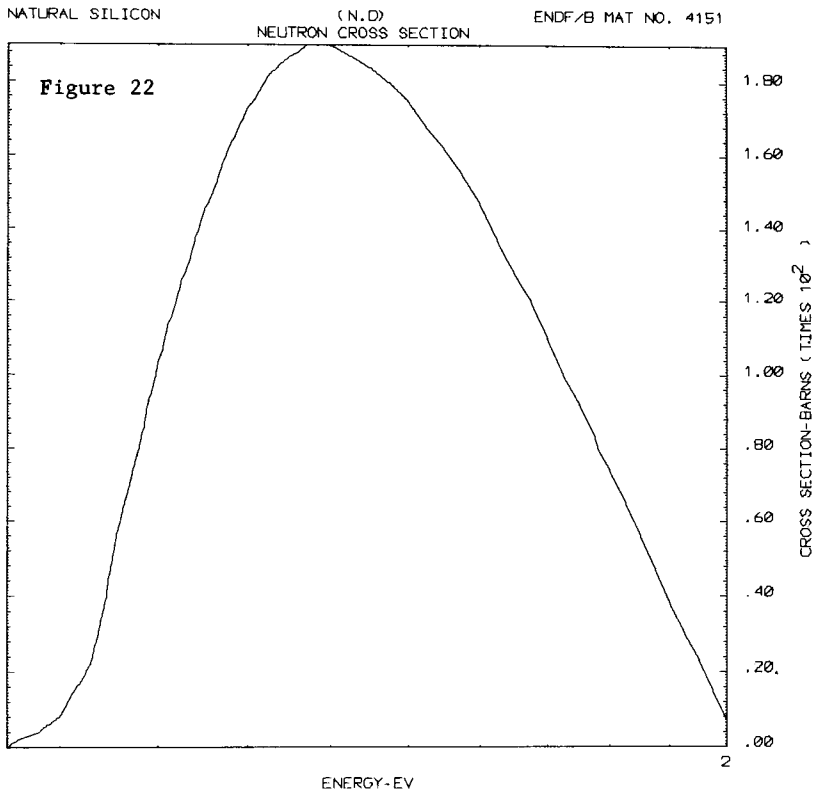

Figure 22

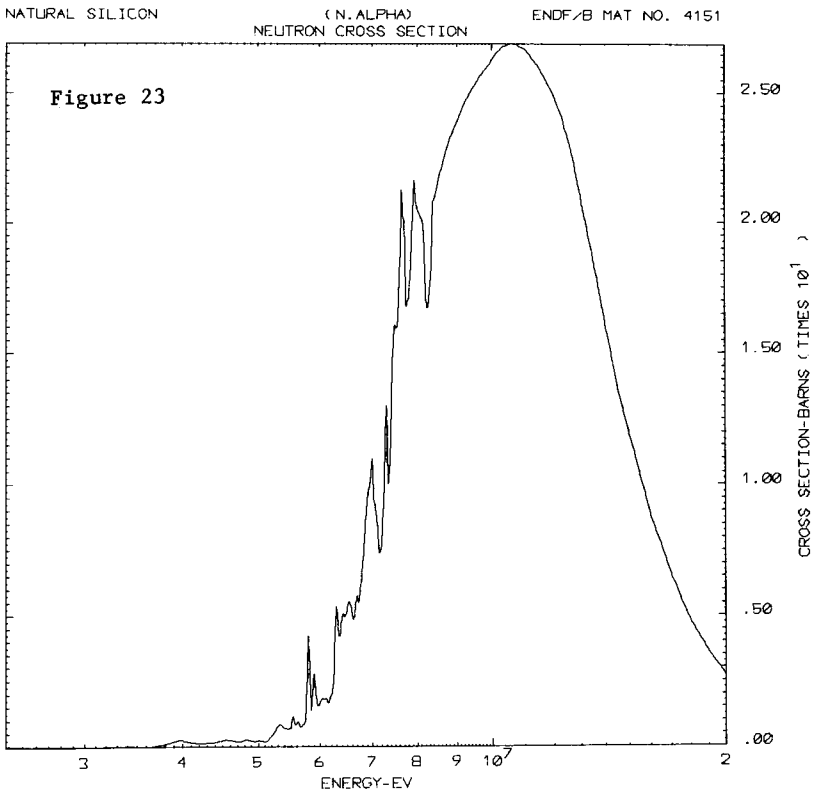

Figure 23

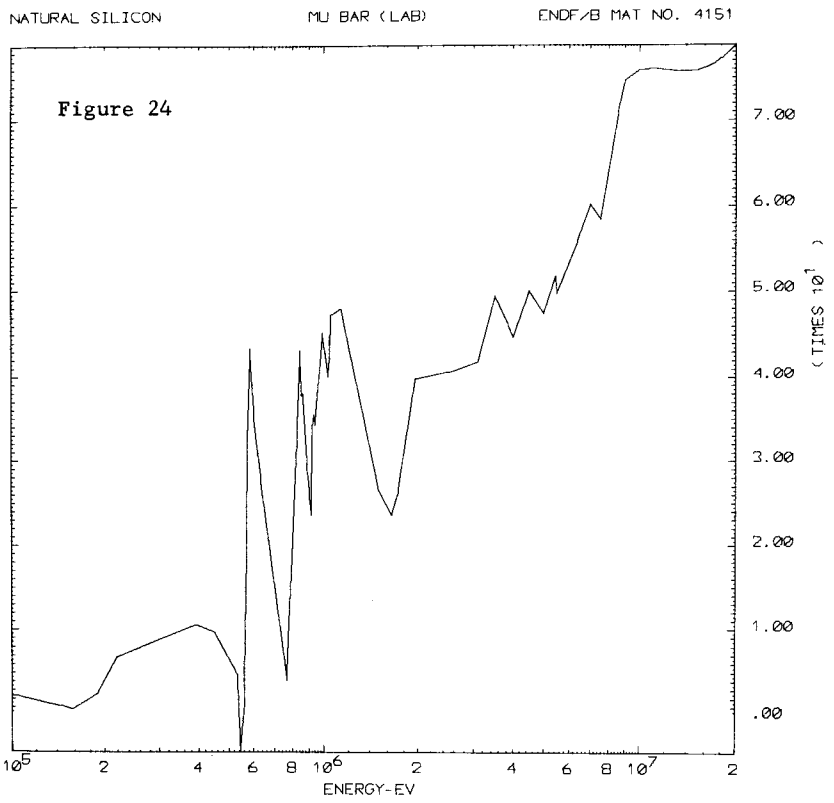

Figure 24

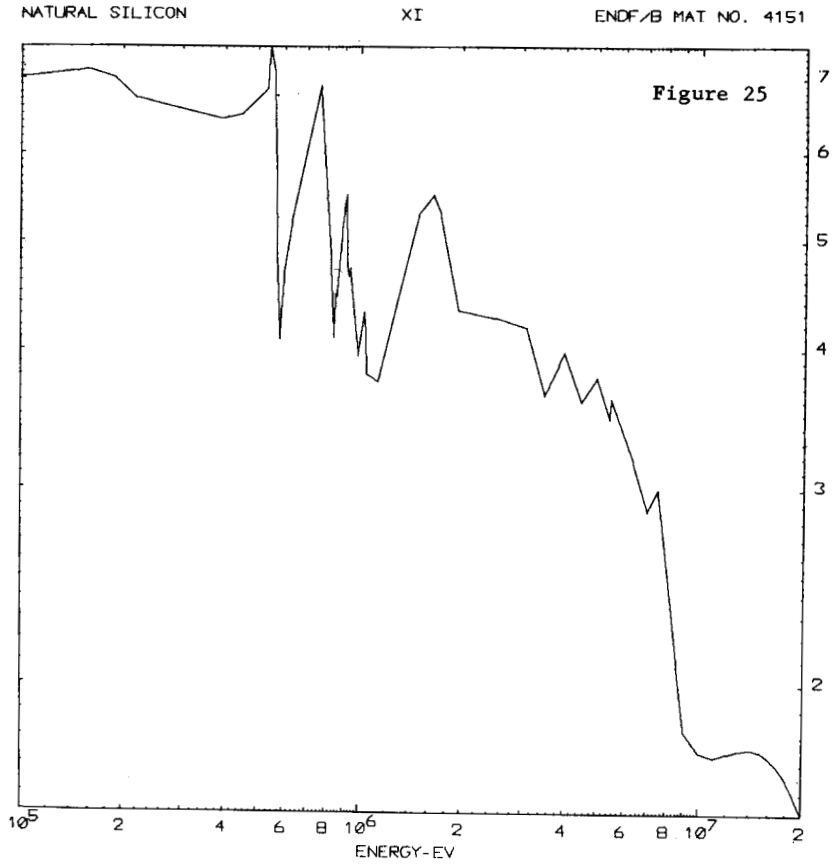

Figure 25

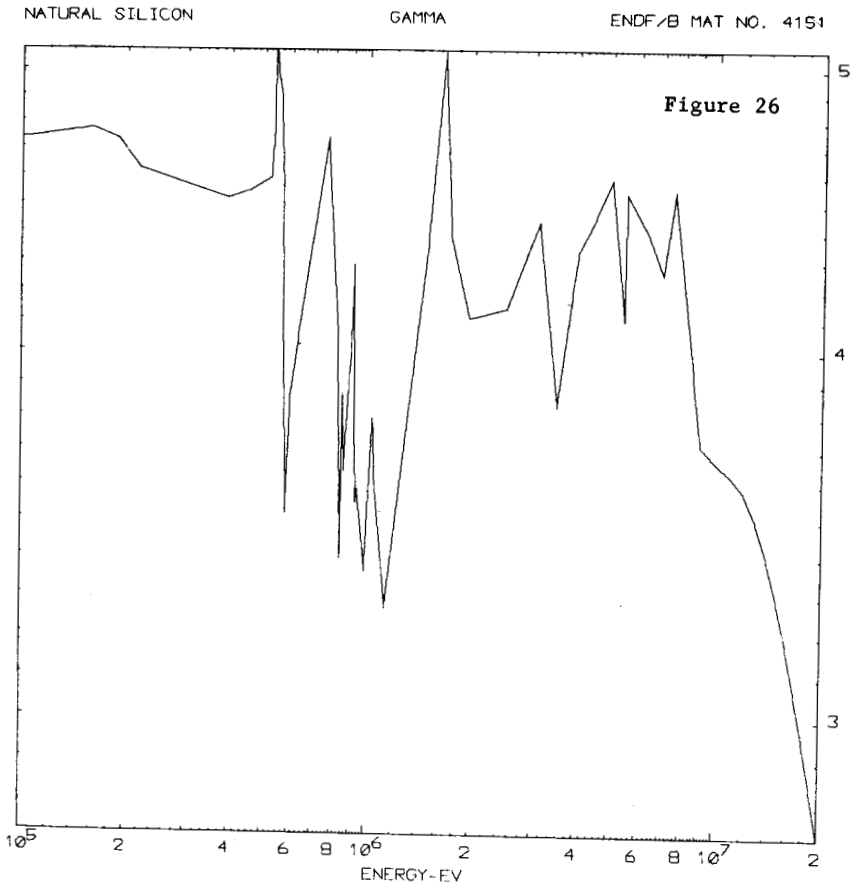

Figure 26

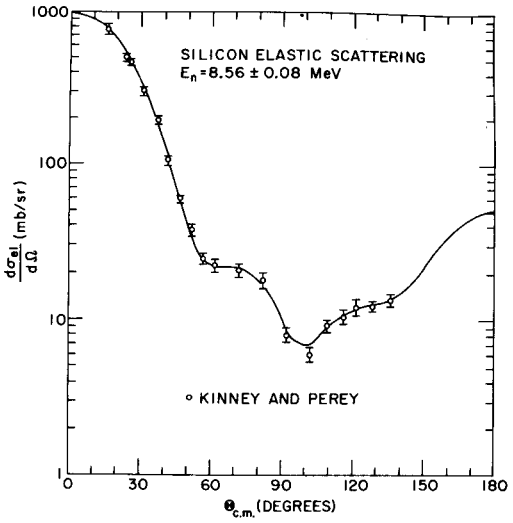

Figure 27

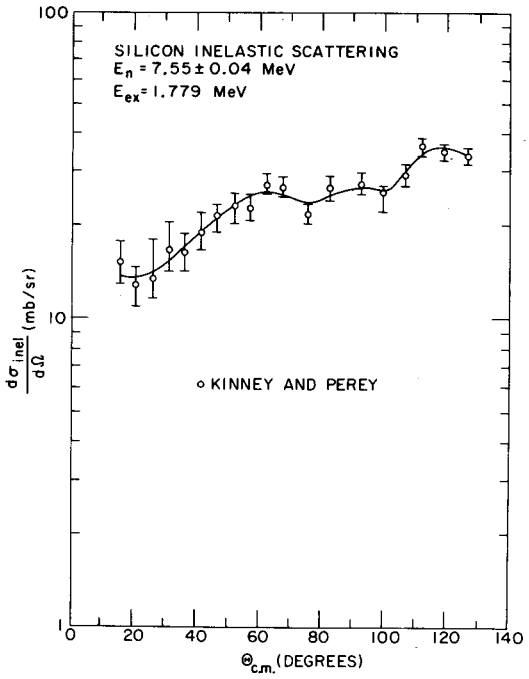

Figure 28

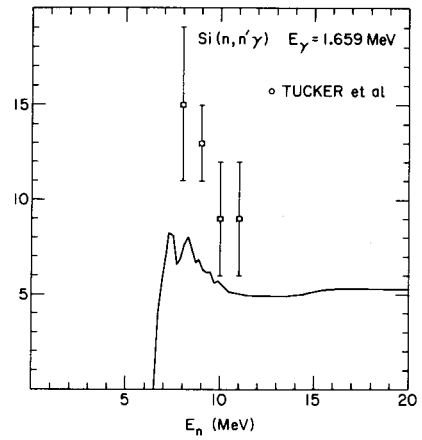

Figure 29

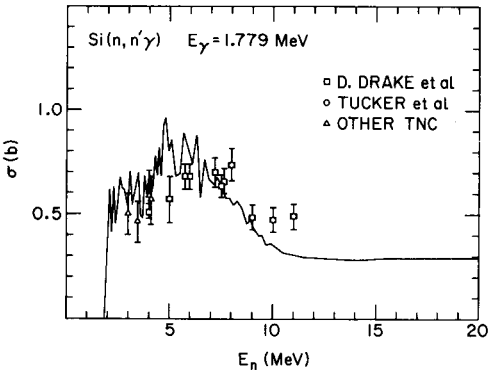

Figure 30

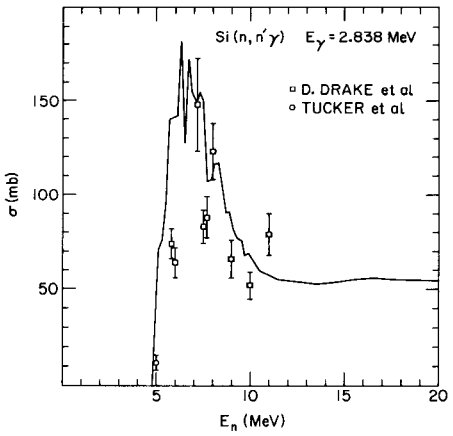

Figure 31

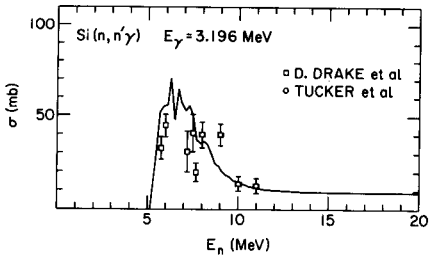

Figure 32

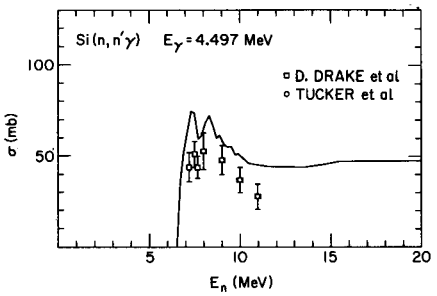

Figure 33

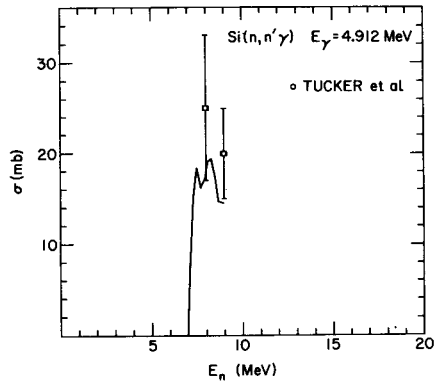

Figure 34

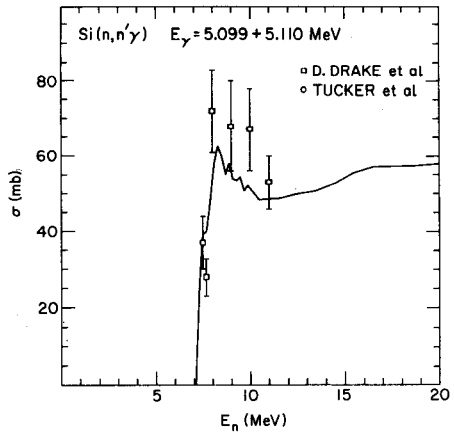

Figure 35

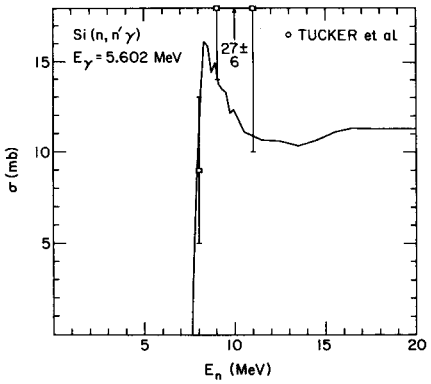

Figure 36

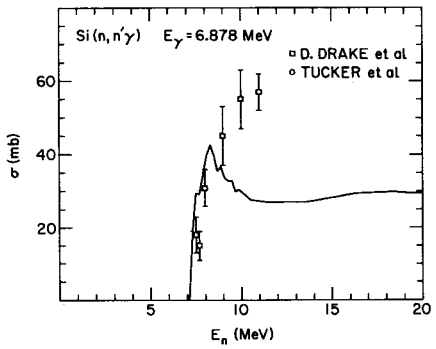

Figure 37

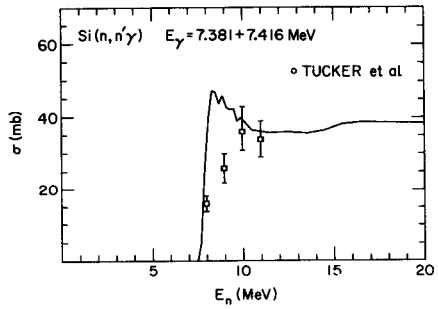

Figure 38

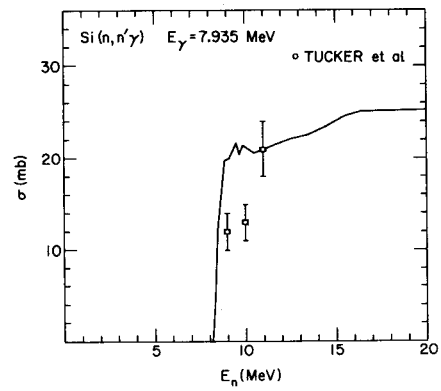

Figure 39